

Detecting Model Misspecification in Bayesian Inverse Problems via Variational Gradient Descent

Qingyang Liu¹, Matthew A. Fisher¹, Zheyang Shen¹,
Katy Tant², Xuebin Zhao³, Andrew Curtis³, Chris. J. Oates^{1,4}

¹Newcastle University, UK

²University of Glasgow, UK

³University of Edinburgh, UK

⁴The Alan Turing Institute, UK

December 2, 2025

Abstract

Bayesian inference is optimal when the statistical model is well-specified, while outside this setting Bayesian inference can catastrophically fail; accordingly a wealth of post-Bayesian methodologies have been proposed. Predictively oriented (PrO) approaches lift the statistical model P_θ to an (infinite) mixture model $\int P_\theta \, dQ(\theta)$ and fit this predictive distribution via minimising an entropy-regularised objective functional. In the well-specified setting one expects the mixing distribution Q to concentrate around the true data-generating parameter in the large data limit, while such singular concentration will typically not be observed if the model is misspecified. Our contribution is to demonstrate that one can empirically detect model misspecification by comparing the standard Bayesian posterior to the PrO ‘posterior’ Q . To operationalise this, we present an efficient numerical algorithm based on variational gradient descent. A simulation study, and a more detailed case study involving a Bayesian inverse problem in seismology, confirm that model misspecification can be automatically detected using this framework.

1 Introduction

Detecting and mitigating model misspecification is a pertinent but difficult issue in Bayesian statistics, where one must consider the full posterior predictive distribution *in lieu* of e.g. plotting a simple scalar residual. The two main approaches to detecting model misspecification (also called *model criticism*) are:

1. *Predictive*: Compare the posterior predictive distribution to held out entries from the dataset [e.g. Gelman et al., 1996, Bayarri and Berger, 2000, Walker, 2013, Moran et al., 2024].
2. *Comparative*: Perform model selection over a set of candidate models in which the current model is contained [e.g. Kass and Raftery, 1995, Wasserman, 2000, Kamary et al., 2014].

In the first case, if the held out data are in some sense ‘unexpected’ under the posterior predictive distribution, this serves as evidence that either the prior or the model may be misspecified. In the second case, if the data strongly support an alternative model, this suggests that the original model may be misspecified. Of course, this is not a true dichotomy and the predictive and comparative approaches are intimately related; for instance, predictive performance is a common criteria for selecting a suitable model [Piironen and Vehtari, 2017, Fong and Holmes, 2020].

For challenging applications, both of these approaches can be impractical. An example of such a challenging application is *seismic travel time tomography* [Curtis and Snieder, 2002, Zhang and Curtis, 2020, Zhao et al., 2022], a regression task where one seeks to reconstruct a subsurface seismic velocity field using measured first arrival times of seismic waves travelling between seismic source and sensor (seismometer) locations. Evaluation of the likelihood and/or its gradient here is associated with a nontrivial computational cost, since the *Eikonal equation*, a partial differential equation describing the high frequency approximation of the wave equation, needs to be solved to estimate the travel times of the first arriving seismic waves. It is worth pointing out that ‘misspecification’ as discussed in this work refers to the suitability of the statistical model for the dataset, rather than any errors that may be present in the physical model for seismic wave travel, though the two issues are of course closely related.

Considering the predictive approach in the seismic tomography context, the spatiotemporal nature of the observations renders the data strongly dependent, representing a challenge in constructing a suitable held-out dataset. Further, while in principle there are solutions to cross-validation for dependent data [e.g. Burman et al., 1994, Rabinowicz and Rosset, 2022], the computational cost associated with performing multiple folds of held-out prediction can render this approach impractical.

Focussing instead on the comparative approach, constructing plausible alternative models requires modifying the physical assumptions underlying the seismic wave propagation. This in turn requires the implementation and optimisation of suitable numerical methods, which demands considerable effort. In the case of model misspecification, there is particular interest in exploring *more* sophisticated models, but without advanced physical insight, constructing such alternatives might be impractical.

The aim of this paper is to propose a *simple, practical and general approach to detecting model misspecification in Bayesian statistics*, and we focus on the seismic travel time tomography problem to demonstrate its potential. Our solution can be considered both a predictive and a comparative approach; predictive because we explicitly assess the predictive performance of the model, and comparative because our principal innovation is to

automate the generation of a candidate model set. To draw an analogy, recall the seminal paper of Kennedy and O’Hagan [2001], where the authors propose augmenting a misspecified physics-based parametric regression function $f_\theta(x)$ with a nonparametric component, i.e. $f_\theta(x) + g(x)$ where $g(x)$ and the parameter θ are to be jointly inferred. In doing so, Kennedy and O’Hagan are in effect automatically generating a set of alternative models without requiring additional physical insight. The approach has been generalised beyond additive misspecification [e.g. to misspecified differential equation models; Alvarez et al., 2013]. However, the drawbacks of this approach are twofold; (i) introducing a nonparametric component increases the data requirement, (ii) any causal predictive power of the model is lost, since the behaviour of the nonparametric component $g(x)$ under intervention cannot be inferred. As such, an alternative approach to automatic generation of candidate models is required.

Our contributions are as follows:

- *Automatic generation of candidate models:* Following similar ideas, in particular *non-parametric maximum likelihood* [Laird, 1978], we lift the statistical model P_θ to an (infinite) mixture model $P_Q := \int P_\theta dQ(\theta)$ as a mechanism to generate an infinite candidate set of alternative models (parametrised by Q), while retaining any causal semantics present in the original statistical model.
- *A predictively oriented ‘posterior’:* Following the *prediction oriented* (PrO) approaches of Masegosa [2020], Sheth and Kharon [2020], Jankowiak et al. [2020a,b], Morningstar et al. [2022], Lai and Yao [2024], Shen et al. [2025], McLatchie et al. [2025], learning of the mixing density Q proceeds based on the performance of the predictive distribution P_Q (in this sense our method is a predictive approach) and is cast as an optimisation task, with the solution being a PrO ‘posterior’ denoted Q_{PrO} .
- *Detecting misspecification:* We propose a direct comparison of the predictive distributions associated with Q_{PrO} and the Bayesian posterior Q_{Bayes} as a general strategy enabling model misspecification to be detected (in this sense our method is a comparative approach). Indeed, McLatchie et al. [2025] proved that in the well-specified setting the predictive distribution associated to Q_{PrO} converges to the true data-generating distribution in the large data limit, in agreement with the predictive distribution associated to Q_{Bayes} , while such agreement is typically not observed when the model is misspecified.
- *Computation as variational gradient descent:* Since Q_{PrO} is defined as the minimiser of a *nonlinear* variational objective, we do not have access to an unnormalised form of the target, and as such standard methods such as Markov chain Monte Carlo (MCMC) cannot be immediately applied. As a solution, we turn to *variational gradient descent* [VGD; Wang and Liu, 2019, Chazal et al., 2025], which is a generalisation of Stein variational gradient descent (SVGD) [Liu and Wang, 2016] to general entropy-regularised objectives. Novel sufficient conditions for the consistency of VGD are presented, than can be verified in the seismology context. Remarkably, sampling from Q_{PrO} can be achieved with a one-line change to standard SVGD.

- *Application to inverse problems:* To demonstrate the applicability of our method in challenging settings, a detailed case study involving seismic travel time tomography is presented. Here our approach is shown to distinguish between the well-specified case and scenarios in which the location of the sensors is misspecified.

Our methods are contained in Section 2, while our empirical assessment is contained in Section 3. A summary of our findings is presented in Section 4, with our proofs and experimental protocol reserved for the Appendix.

2 Methods

The variational formulation of Bayesian updating and the related PrO approach are recalled in Section 2.1. The VGD methodology is presented in Section 2.2. Novel theoretical analysis of VGD is required to establish its validity in our context, and this is presented in Section 2.3. Our implementation is described in Section 2.4 and our overall framework is summarised in Section 2.5.

2.1 Bayesian and Predictively Oriented Approaches

Let P_θ denote a statistical model whose density p_θ we assume to exist on \mathbb{R}^d . Let y denote the dataset. In what follows, motivated by our seismic tomography case study, we focus on regression modelling, where responses $\{y_i\}_{i=1}^n$ are conditionally independent given covariates $\{x_i\}_{i=1}^n$, so that

$$\log p_\theta(y) = \sum_{i=1}^n \log p_\theta(y_i|x_i)$$

where the dependence on the covariates x_i is made explicit. However it should be noted that our methods are applicable beyond the regression context.

Standard Bayesian Posterior Let $\mathcal{P}(\mathbb{R}^d)$ denote the set of distributions¹ on \mathbb{R}^d . Let $Q \ll Q_0$ denote that Q is absolutely continuous with respect to Q_0 , and dQ/dQ_0 the Radon–Nikodym density of Q with respect to Q_0 . For $Q \ll Q_0$, the Kullback–Leibler divergence (KLD) is defined as $\text{KLD}(Q||Q_0) := \int \log(dQ/dQ_0) dQ$, while for $Q \not\ll Q_0$ we set $\text{KLD}(Q||Q_0) = \infty$. Recall the variational characterisation of the standard Bayesian posterior due to Zellner [1988]:

$$Q_{\text{Bayes}} := \arg \min_{Q \in \mathcal{P}(\mathbb{R}^d)} - \sum_{i=1}^n \int \log p_\theta(y_i|x_i) dQ(\theta) + \text{KLD}(Q||Q_0)$$

where $Q_0 \in \mathcal{P}(\mathbb{R}^d)$ is the prior distribution [see also e.g. Knoblauch et al., 2022]. For the integral to be well-defined, i.e. for $\theta \mapsto -\log p_\theta(y)$ to be Q -integrable for all $Q \in \mathcal{P}(\mathbb{R}^d)$, it is sufficient for $\theta \mapsto p_\theta(y)$ to be bounded.

¹Measurability is implicitly assumed in this manuscript.

Predictively Oriented Posterior The PrO approaches of Masegosa [2020], Sheth and Khardon [2020], Jankowiak et al. [2020a,b], Morningstar et al. [2022], Lai and Yao [2024], Shen et al. [2025], McLatchie et al. [2025] were developed with the aim of avoiding over-confident predictions when the statistical model is misspecified. These approaches lift the original parametric model P_θ into a mixture model P_Q , with density

$$p_Q(y_i|x_i) = \int p_\theta(y_i|x_i) dQ(\theta),$$

and then attempt to learn Q by minimising an entropy-regularised objective functional. For the purpose of this paper we measure the suitability of Q using the (relative) entropy-regularised mixture log-likelihood

$$Q_{\text{PrO}} := \arg \min_{Q \in \mathcal{P}(\mathbb{R}^d)} - \sum_{i=1}^n \log p_Q(y_i|x_i) + \text{KLD}(Q||Q_0). \quad (1)$$

This can be viewed as an entropy-regularised form of *nonparametric maximum likelihood* [Laird, 1978]; the entropic regularisation is a key ingredient, since otherwise the solution will be atomic [Lindsay, 1995, e.g. Theorem 21 in Chapter 5]. For other related work see the discussion in Shen et al. [2025], McLatchie et al. [2025].

Since the variational formulation (1) is non-standard, we should first ask if Q_{PrO} is well-defined. Let $\mathcal{P}_\alpha(\mathbb{R}^d)$ denote the subset of $\mathcal{P}(\mathbb{R}^d)$ for which moments of order α exist. The proof of the following result is contained in Section A.2:

Proposition 1 (Q_{PrO} is well-defined). *Let Q_0 admit a positive density q_0 on \mathbb{R}^d . Let $p_\theta(y_i|x_i)$ be bounded in θ for each (x_i, y_i) in the dataset. Then there exists a unique solution to (1). Further, if $Q_0 \in \mathcal{P}_\alpha(\mathbb{R}^d)$ then $Q_{\text{PrO}} \in \mathcal{P}_\alpha(\mathbb{R}^d)$.*

The benefit of lifting to a mixture model is as follows: If the original statistical model P_θ was well-specified, so that there really was a correct parameter θ_\star , then we can hope Q_{PrO} concentrates around θ_\star (i.e. collapses to a mixture model with a single mixture component). Likewise one would expect vanishing posterior uncertainty in the standard Bayesian context. Inspecting whether the learned Q_{PrO} agrees with the standard Bayesian posterior Q_{Bayes} can therefore provide a useful validation that the model is well-specified. On the other hand, if the original statistical model was misspecified, then we expect Q_{PrO} to learn a non-trivial mixture model, assuming such a mixture provides a better explanation of the dataset than any single instance of P_θ could. That is, Q_{PrO} is able to *adapt* to the level of model misspecification, in a way that standard Bayesian inference cannot. These intuitions for the asymptotic behaviour of Q_{PrO} are confirmed in the recent detailed theoretical treatment in McLatchie et al. [2025]. An empirical demonstration of the effectiveness of this approach is the subject of Section 3; the remainder of this section addresses the key practical question of how to calculate Q_{PrO} in (1).

Remark 1 (Learning rate-free). *Note that, unlike generalised Bayesian methods [Bissiri et al., 2016, Knoblauch et al., 2022] and in contrast to the earlier work on PrO approaches*

in Lai and Yao [2024], Shen et al. [2025], McLatchie et al. [2025], no learning rate appears in (1) since the data term is automatically on the correct scale (being a log-likelihood, it is measured in nats). Earlier works introduced a learning rate λ in the form of $\lambda \times \text{KLD}(Q||Q_0)$ to accommodate other choices of data-dependent loss, such as maximum mean discrepancy, for which the units are not directly comparable. Selection of learning rates is known to be difficult [Wu and Martin, 2023] and it is therefore advantageous that these can be avoided.

2.2 Variational Gradient Descent

An immediate question is *how to solve* (1)? Since the parameter of the mixture model is Q , it is unclear how to proceed; Q lives in $\mathcal{P}(\mathbb{R}^d)$ which is not a vector space, making it unclear how to apply operations such as taking a gradient with respect to Q . To resolve this problem we consider a general entropy-regularised variational objective

$$\mathcal{J}(Q) := \mathcal{L}(Q) + \text{KLD}(Q||Q_0), \quad (2)$$

which accommodates both Q_{Bayes} and Q_{PrO} by taking the loss function to be either

$$\mathcal{L}_{\text{Bayes}}(Q) = - \int \sum_{i=1}^n \log p_{\theta}(y_i|x_i) \, dQ(\theta), \quad \text{or} \quad \mathcal{L}_{\text{PrO}}(Q) = - \sum_{i=1}^n \log \int p_{\theta}(y_i|x_i) \, dQ(\theta), \quad (3)$$

which differ only in the order in which the integral and the logarithm are performed. Our aim is a rigorous notion of gradient descent that can be applied to (relative) entropy-regularised objective in (2).

Remark 2 (Established numerical methods for (2)). *One could approximate Q_{PrO} using established numerical methods designed for variational tasks, the most well-studied of which is mean field Langevin dynamics (MFLD) [Del Moral, 2013]. However, due to computational limitations, numerical methods based on long-run ergodic averages are generally avoided in seismic tomography in favour of more efficient particle-based algorithms such as SVGD [see e.g. Zhang and Curtis, 2020, Zhang et al., 2023]. Here we propose to approximate both Q_{Bayes} and Q_{PrO} using VGD, noting that in the first case VGD coincides with SVGD due to the linear form of the loss function $\mathcal{L}_{\text{Bayes}}$. In fact, we will see in Section 2.5 that applying VGD to Q_{PrO} requires only a one line-change to standard SVGD.*

Variational Gradient The notion of a gradient that we will need is a *variational gradient*. For a suitably regular functional $\mathcal{F} : \mathcal{P}(\mathbb{R}^d) \rightarrow \mathbb{R}$, the *first variation* at $Q \in \mathcal{P}(\mathbb{R}^d)$ is defined as a map $\mathcal{F}'(Q) : \mathbb{R}^d \rightarrow \mathbb{R}$ such that $\lim_{\epsilon \rightarrow 0} \frac{1}{\epsilon} \{\mathcal{F}(Q + \epsilon\chi) - \mathcal{F}(Q)\} = \int \mathcal{F}'(Q) \, d\chi$ for all perturbations χ of the form $\chi = Q' - Q$ with $Q' \in \mathcal{P}(\mathbb{R}^d)$; note that if it exists, the first variation is unique up to an additive constant. Given a functional $\mathcal{F}(Q)$ we define $\nabla_{\text{V}}\mathcal{F}(Q)(\theta) := \nabla_{\theta}\mathcal{F}'(Q)(\theta)$ where $\mathcal{F}'(Q)$ is the first variation of \mathcal{F} at Q [Chazal et al., 2025,

Definition 1]. For the loss functions in (3) we have

$$\nabla_V \mathcal{L}_{\text{Bayes}}(Q)(\theta) = - \sum_{i=1}^n \nabla_{\theta} \log p_{\theta}(y_i|x_i) \quad (4)$$

$$\nabla_V \mathcal{L}_{\text{PrO}}(Q)(\theta) = - \sum_{i=1}^n w_{\theta}^Q(y_i|x_i) \nabla_{\theta} \log p_{\theta}(y_i|x_i), \quad w_{\theta}^Q(y_i|x_i) := \frac{p_{\theta}(y_i|x_i)}{p_Q(y_i|x_i)}, \quad (5)$$

see Proposition 4 in Section A.1. Note that (5) can be seen as a weighted version of (4), which agrees when $Q = \delta_{\theta}$ is a Dirac distribution at $\theta \in \mathbb{R}^d$.

Computing Directional Derivatives Let $T_{\#}Q$ denote the distribution of $T(X)$ where $X \sim Q$. Consider the directional derivatives

$$\left. \frac{d}{d\epsilon} \mathcal{J}((I_d + \epsilon v)_{\#}Q) \right|_{\epsilon=0}$$

as specified by a suitable vector field $v : \mathbb{R}^d \rightarrow \mathbb{R}^d$, where I_d is the identity map on \mathbb{R}^d . For the purpose of optimisation, we seek a vector field v for which the rate of decrease in \mathcal{J} is maximised. To this end, letting

$$\mathcal{T}_Q v(\theta) := [(\nabla \log q_0)(\theta) - \nabla_V \mathcal{L}(Q)(\theta)] \cdot v(\theta) + (\nabla \cdot v)(\theta),$$

it follows from the fundamental theorem of calculus [see e.g. Section 3.2.2.2 of Chazal et al., 2025] that

$$\left. \frac{d}{d\epsilon} \mathcal{J}((I_d + \epsilon v)_{\#}Q) \right|_{\epsilon=0} = - \int \mathcal{T}_Q v(\theta) dQ(\theta). \quad (6)$$

That is, the directional derivative of the objective \mathcal{J} in (2) can be expressed as an explicit Q -dependent linear functional applied to the vector field.

Following the Directions of Steepest Descent Next, following the same logic as Wang and Liu [2019], we pick the vector field v_Q from the unit ball of an appropriate Hilbert space for which the magnitude of the negative gradient in (6) is maximised. For a multivariate function, let $\partial_{i,j}$, ∇_i , etc, indicate the action of the differential operators with respect to the i th argument. Letting \mathcal{H}_k denote the reproducing kernel Hilbert space (RKHS) associated to a symmetric positive semi-definite kernel $k : \mathbb{R}^d \times \mathbb{R}^d \rightarrow \mathbb{R}$, we seek $v_Q \in \mathcal{H}_k^d$, the d -fold Cartesian product, which leads to

$$v_Q(\cdot) \propto \int \{k(\theta, \cdot)(\nabla \log q_0 - \nabla_V \mathcal{L}(Q))(\theta) + \nabla_1 k(\theta, \cdot)\} dQ(\theta). \quad (7)$$

To numerically approximate this gradient descent, we initialise $\{\theta_j^0\}_{j=1}^N$ as independent samples from μ_0 at time $t = 0$ and then update $\{\theta_j^t\}_{j=1}^N$ deterministically, via the coupled system of ordinary differential equations (ODEs)

$$\frac{d\theta_i^t}{dt} = \frac{1}{N} \sum_{j=1}^N k(\theta_i^t, \theta_j^t) (\nabla \log q_0 - \nabla_V \mathcal{L}(Q_N^t))(\theta_j^t) + \nabla_1 k(\theta_j^t, \theta_i^t), \quad Q_N^t := \frac{1}{N} \sum_{j=1}^N \delta_{\theta_j^t} \quad (8)$$

up to a time horizon T . The first consistency result in this context was established in Proposition 3 of Chazal et al. [2025], who called the algorithm *variational gradient descent* (VGD). For Q_{Bayes} , VGD coincides with SVGD [Liu and Wang, 2016] and the sharpest convergence analysis of SVGD to-date appears in Banerjee et al. [2025]. Unfortunately the assumptions made in Chazal et al. [2025] are too restrictive to handle Q_{PrO} . To resolve this issue, a novel convergence guarantee for VGD in the context of Q_{PrO} is presented next.

2.3 Consistency of VGD

To discuss the consistency of VGD we need to specify in what sense the approximation is consistent. To this end, let $\mathcal{B}_k^d = \{v \in \mathcal{H}_k^d : \sum_i \|v_i\|_{\mathcal{H}_k}^2 \leq 1\}$ denote the unit ball in \mathcal{H}_k^d . Let $\mathcal{L}^1(Q) := \{f : \mathbb{R}^d \rightarrow \mathbb{R} : \int \|f(x)\| dQ(x) < \infty\}$ denote² the set of Q -integrable functions on \mathbb{R}^d . Let f_- denote the negative part $f_- : x \mapsto \min\{0, f(x)\}$ of a function f . The kernel gradient discrepancy (KGD) [Chazal et al., 2025, Definition 4]

$$\text{KGD}_k(Q) := \sup_{\substack{v \in \mathcal{B}_k^d \text{ s.t.} \\ (\mathcal{T}_Q v)_- \in \mathcal{L}^1(Q)}} \left| \int \mathcal{T}_Q v(\theta) dQ(\theta) \right| \quad (9)$$

can be interpreted as a gradient norm for \mathcal{J} using (6); a small KGD indicates that Q is close to being a stationary point (and in particular a minimiser, due to convexity) of \mathcal{J} . The precise topologies induced on $\mathcal{P}(\mathbb{R}^d)$ by KGD can be weaker or stronger depending on how the kernel k is selected; this is discussed in detail in Chazal et al. [2025] but such discussion is beyond the scope of the present work.

Let $C^r(\mathbb{R}^d)$ denote the set of r times continuously differentiable functionals on \mathbb{R}^d . The proof of the following result is contained in Section A.3:

Proposition 2 (Consistency of VGD for Q_{PrO}). *Assume that:*

1. (Initialisation) μ_0 has bounded support, and has a density that is $C^2(\mathbb{R}^d)$.
2. (Kernel) k is $C^3(\mathbb{R}^d)$ in each argument with the growth of $(\theta, \vartheta) \mapsto \|\nabla_1 k(\theta, \vartheta)\|$ at most linear, and $\sup_{\theta \in \mathbb{R}^d} |\Delta_1 k(\theta, \theta)| < \infty$.
3. (Regularisation) $\log q_0 \in C^3(\mathbb{R}^d)$ with the growth of $\theta \mapsto k(\theta, \theta) \|\nabla \log q_0(\theta)\|$ at most linear, and $\sup_{\theta \in \mathbb{R}^d} k(\theta, \theta) |\Delta \log q_0(\theta)| < \infty$.

²This should not be confused with the notation \mathcal{L} for the loss function in (2).

Algorithm 1 Variational Gradient Descent for Q_{Bayes} and Q_{PrO}

Require: $\{\theta_j^0\}_{j=1}^N \subset \mathbb{R}^d$ (initial particles), $\epsilon > 0$ (step size)

for $t = 0, \dots, T - 1$ **do**

$$w_\theta^t(y_i|x_i) := p_\theta(y_i|x_i) / (\frac{1}{N} \sum_{r=1}^N p_{\theta_r^t}(y_i|x_i))$$

$$s_t(\theta) := \begin{cases} (\nabla \log q_0)(\theta) + \sum_{i=1}^n \nabla_\theta \log p_\theta(y_i|x_i) & \text{to target } Q_{\text{Bayes}} \\ (\nabla \log q_0)(\theta) + \sum_{i=1}^n w_\theta^t(y_i|x_i) \nabla_\theta \log p_\theta(y_i|x_i) & \text{to target } Q_{\text{PrO}} \end{cases}$$

for $j = 1, \dots, N$ **do**

$$\theta_j^{t+1} \leftarrow \theta_j^t + \frac{\epsilon}{N} \sum_{r=1}^N \nabla_1 k(\theta_r^t, \theta_j^t) + s_t(\theta_r^t) k(\theta_r^t, \theta_j^t)$$

end for

end for

4. (Regularity of P_θ) $\theta \mapsto p_\theta(y_i|x_i)$ is positive, bounded and $C^3(\mathbb{R}^d)$ with

$$a. \sup_{\theta \in \mathbb{R}^d} \sqrt{k(\theta, \theta)} \frac{\|\nabla_\theta p_\theta(y_i|x_i)\|}{p_\theta(y_i|x_i)} < \infty$$

$$b. \sup_{\theta \in \mathbb{R}^d} k(\theta, \theta) \frac{\Delta_\theta p_\theta(y_i|x_i)}{p_\theta(y_i|x_i)} < \infty$$

for each (x_i, y_i) in the dataset.

Then the dynamics defined in (8) with $\mathcal{L} = \mathcal{L}_{\text{PrO}}$ satisfies

$$\frac{1}{T} \int_0^T \mathbb{E}[\text{KGD}_k^2(Q_N^t)] dt \leq \frac{\text{KLD}(\mu_0 || \rho_{\mu_0})}{T} + \frac{C_k}{N}$$

for some finite constant C_k , where ρ_{μ_0} denotes the distribution with density proportional to $q_0(\theta) \exp(-\mathcal{L}'_{\text{PrO}}(\mu_0)(\theta))$.

Proposition 2 provides the first consistency guarantee for VGD in the setting of \mathcal{L}_{PrO} .

Remark 3 (On the assumptions). *Our assumptions in Proposition 2 rule out models for which the Fisher score $\theta \mapsto \nabla_\theta \log p_\theta(y_i|x_i)$ is unbounded when the kernel is translation-invariant. This is a strong assumption in general, but it is satisfied in seismic tomography, where the Fisher score asymptotically vanishes as a result of the wave propagation model being physics-constrained³. This is not a unique property of seismic tomography, and we expect that many other physics-constrained inverse problems would similarly satisfy our regularity requirement.*

2.4 Implementation of VGD

For the purposes of this paper, computation of both Q_{Bayes} and Q_{PrO} was performed using a time discretisation of VGD as described in Algorithm 1. In each case, Algorithm 1 starts

³Equivalently, physical considerations dictate that model parameters can be confined to a compact set (and then reparametrised back to \mathbb{R}^d), as done in Zhang et al. [2023].

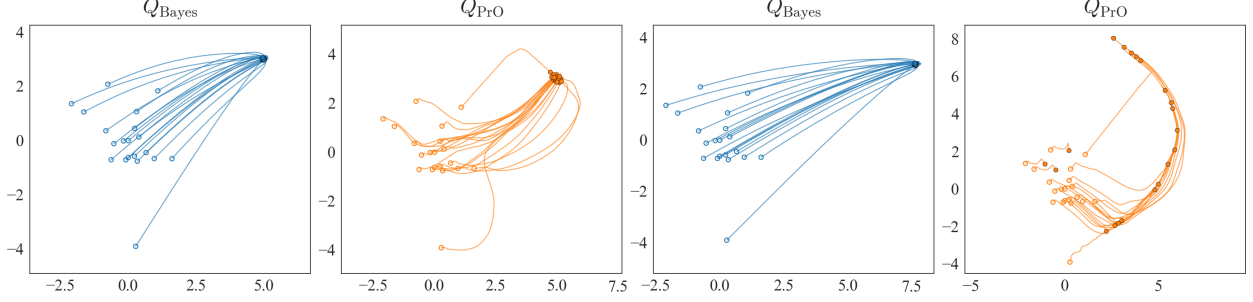


Figure 1: Illustrating the convergence of variational gradient descent (VGD) in the context of the two-dimensional example discussed in Section 3.1. The hollow circular markers depict initial particle locations $\{\theta_j^0\}_{j=1}^N$, lines represent trajectories at intermediate times $\{\theta_j^t\}_{j=1}^N$, and filled circular markers depict final locations $\{\theta_j^T\}_{j=1}^N$. The left and centre-left panels correspond to Q_{Bayes} and Q_{PrO} in a setting where the statistical model is well-specified, while the centre-right and right panels correspond to Q_{Bayes} and Q_{PrO} in a setting where the statistical model is misspecified. Here $N = 20$ particles were used.

by initialising N particles and then iteratively updating the particles according to an Euler discretisation of the ODEs (8) with step size $\epsilon > 0$ to be specified. After T time steps, the collection of particles represents an empirical approximation to either Q_{Bayes} or Q_{PrO} . It is worth reiterating that computation of Q_{PrO} requires a one-line change to existing implementations of SVGD, and that Q_{Bayes} and Q_{PrO} can be computed in parallel. The rapid convergence of VGD in a toy two-dimensional setting is displayed in Figure 1.

2.5 Summary of Approach

Our approach, in a nutshell, is to calculate both Q_{Bayes} and Q_{PrO} and to see if they are ‘sufficiently similar’ or not. If these distributions are substantially different, we interpret this as evidence that the model may be misspecified.

An obvious question at this point is *how to decide whether Q_{Bayes} and Q_{PrO} are sufficiently similar?* If the model is well-specified, Q_{Bayes} concentrates around the true parameter θ_* . Thus we are interested in whether Q_{PrO} also appears to concentrate around θ_* or not. Unfortunately, it is not the case that Q_{Bayes} and Q_{PrO} concentrate at the same rate; it is well-known that Q_{Bayes} concentrates at a rate $n^{-1/2}$, while it appears that a slower rate is typical for Q_{PrO} [McLatchie et al., 2025]. The lack of a complete understanding of the concentration of Q_{PrO} limits the extent to which the above question can be answered. Instead, we compare the predictive distributions $P_{Q_{\text{Bayes}}}(\cdot|x) = \int P_\theta(\cdot|x) dQ_{\text{Bayes}}(\theta)$ and $P_{Q_{\text{PrO}}}(\cdot|x) = \int P_\theta(\cdot|x) dQ_{\text{PrO}}(\theta)$ (to simplify notation in this paragraph, we will denote these predictive distributions in shorthand as P_{Bayes} and P_{PrO} , and the dependence on x will be left implicit). In the well-specified case, and for any metric \mathcal{D} for which $\mathcal{D}(P_n, P_0) \rightarrow 0$ whenever $\text{KLD}(P_n||P_0) \rightarrow 0$, it can be shown⁴ that $\mathbb{E}[\mathcal{D}(P_{\text{PrO}}, P_{\text{Bayes}})] \rightarrow 0$ as $n \rightarrow \infty$. That is, if the number of data n is large

⁴This follows from Corollary 1 in McLatchie et al. [2025], who showed that $\mathbb{E}[\text{KLD}(P_{\text{PrO}}||P_0) -$

enough then P_{PrO} and P_{Bayes} should be almost identical when the model is well-specified. Conversely, if Q_{PrO} does not concentrate around the same parameter θ_* as Q_{Bayes} , then we can expect to detect this as an irreducible difference between the predictive distributions P_{PrO} and P_{Bayes} .

To operationalise this idea, we propose to construct an approximate null distribution for the (average squared) maximum mean discrepancy (MMD)

$$D(\{(x_i, y_i)\}_{i=1}^n) \equiv \mathcal{D}(P_{\text{PrO}}, P_{\text{Bayes}}) = \frac{1}{n} \sum_{i=1}^n \text{MMD}^2(P_{\text{PrO}}(\cdot|x_i), P_{\text{Bayes}}(\cdot|x_i)), \quad (10)$$

under the hypothesis that the statistical model is well-specified. To do so, we let θ_n be the mean of Q_{Bayes} ⁵ and then repeatedly compute $D(\{(x_i, \tilde{y}_i)\}_{i=1}^n)$ based on synthetic datasets where \tilde{y}_i is simulated from $P_{\theta_n}(\cdot|x_i)$. The actual value $D(\{(x_i, y_i)\}_{i=1}^n)$ can be compared to the null distribution so-obtained. While one could formally report a p -value and investigate the asymptotic consistency of such a test [e.g. by extending Key et al., 2021, to the case where data are conditionally independent], we limit scope and simply view (10) as a diagnostic in the present work. A systematic empirical investigation of this approach is contained in Section 3.

3 Empirical Assessment

Preempting our application to seismic tomography, our focus in this section is on Gaussian regression models of the form

$$p_{\theta}(y_i|x_i) = \frac{1}{\sqrt{2\pi \det(\Sigma)}} \exp\left(-\frac{1}{2}\|\Sigma^{-\frac{1}{2}}(y_i - f_{\theta}(x_i))\|^2\right), \quad (11)$$

for responses $\{y_i\}_{i=1}^n$ conditional on covariates $\{x_i\}_{i=1}^n$, with known measurement error covariance matrix Σ and unknown regression parameters $\theta \in \mathbb{R}^d$. Our interest is in settings where the parametric regression function $f_{\theta}(x)$ could be misspecified. Proceeding with Bayesian inference would be problematic if $f_{\theta}(x)$ is indeed misspecified, since increasing the number of data n would cause the posterior to collapse onto a single ‘best’ parameter θ_* and the predictions from the model will collapse also to f_{θ_*} , i.e. the predictions are simultaneously high-confidence and incorrect.

Our principal interest is in whether a comparison of Q_{Bayes} and Q_{PrO} enables misspecification to be detected. Section 3.1 reports a detailed empirical investigation in a controlled

$\text{KLD}(P_{\text{Bayes}}||P_0) \rightarrow 0$ where P_0 is the true data distribution. Combining this with the predictive consistency of Bayesian inference in the well-specified case, i.e. $\mathbb{E}[\text{KLD}(P_{\text{Bayes}}||P_0)] \rightarrow 0$, we deduce that $\mathbb{E}[\text{KLD}(P_{\text{PrO}}||P_0)] \rightarrow 0$. Since Kullback–Leibler is not a metric we cannot deduce anything about e.g. $\text{KLD}(P_{\text{PrO}}||P_{\text{Bayes}})$, but from our assumptions on \mathcal{D} we can apply the triangle inequality $\mathcal{D}(P_{\text{PrO}}, P_{\text{Bayes}}) \leq \mathcal{D}(P_{\text{PrO}}, P_0) + \mathcal{D}(P_{\text{Bayes}}, P_0) \rightarrow 0$ to yield the claimed result.

⁵The posterior mean θ_n could be replaced with any estimator of θ that is consistent when the model is well-specified. In the special case where θ_n is replaced by a sample from Q_{Bayes} , our approach is similar to a *posterior predictive check* with D as the test statistic [Rubin, 1984, Gelman et al., 1996].

setting where data are generated from a simple known regression model, while a challenging application to seismic tomography is presented in Section 3.2. In both cases the statistical model takes the form (11), and we can interpret the sufficient conditions for the convergence of VGD in Proposition 2 this context. The proof of the following result is contained in Section A.4:

Proposition 3 (Regularity conditions for Gaussian regression model (11)). *Let P_θ be the Gaussian regression model in (11), and let k be a symmetric positive semi-definite kernel for which $f_\theta(x_i)$, $\sqrt{k(\theta, \theta)}\nabla_\theta f_\theta(x_i)$, and $k(\theta, \theta)\Delta_\theta f_\theta(x_i)$ are bounded in θ for each x_i in the dataset. Then Item 4 of Proposition 2 is satisfied.*

Although the assumptions of Proposition 3 are too strong for applications such as linear regression, where the regression function $f_\theta(x) = \theta \cdot x$ can be unbounded, for physics-constrained inverse problems (including our seismic tomography case study in Section 3.2) the boundedness requirements are typically satisfied.

3.1 Simulation Study

The aim of this section is to empirically assess whether our methods can detect when the regression function $f_\theta(x)$ is misspecified. To this end, we considered several toy regression tasks of the form (11), varying both the size of the dataset, the dimension of the parameter vector, and the extent to which the data-generating distribution departs from the regression model. Full details of our simulation setup are reserved for Section B.

Results are presented in Figure 2, where each row corresponds to a different regression model. It is visually apparent that the spread of the posterior predictive P_{PrO} is similar to that of P_{Bayes} when the model is well-specified, and much wider than the spread of P_{Bayes} when the model is misspecified. This difference in the misspecified setting occurs because the standard Bayesian posterior Q_{Bayes} is destined to concentrate on a single ‘least bad’ parameter θ_\star as the size of the dataset is increased, while the predictively oriented posterior Q_{PrO} is able to adapt to the level of model misspecification, resulting in an irreducible uncertainty in Q_{PrO} that does not vanish as the number of data is increased. The parameter posteriors Q_{Bayes} and Q_{PrO} themselves for these examples are presented in Figure 5 of Section B.4, where we also verify the convergence of the VGD algorithm used to obtain these results, as measured using the KGD in (9).

The distribution of the test statistic D under the ‘well-specified null’ described in Section 2.5, alongside the actual realised value of D , are also displayed in Figure 2. It can be seen that the realised value of D is far into the tail of the null distribution when data are not generated from the statistical model, meaning that the test statistic is able to detect that the statistical model is misspecified. Empirically, a larger sample size n increases the power of the test, as expected; see Figure 6 in Section B.4. Conversely, the detection of model misspecification is more challenging when a large number of parameters θ are being estimated; see Figure 7 in Section B.4.

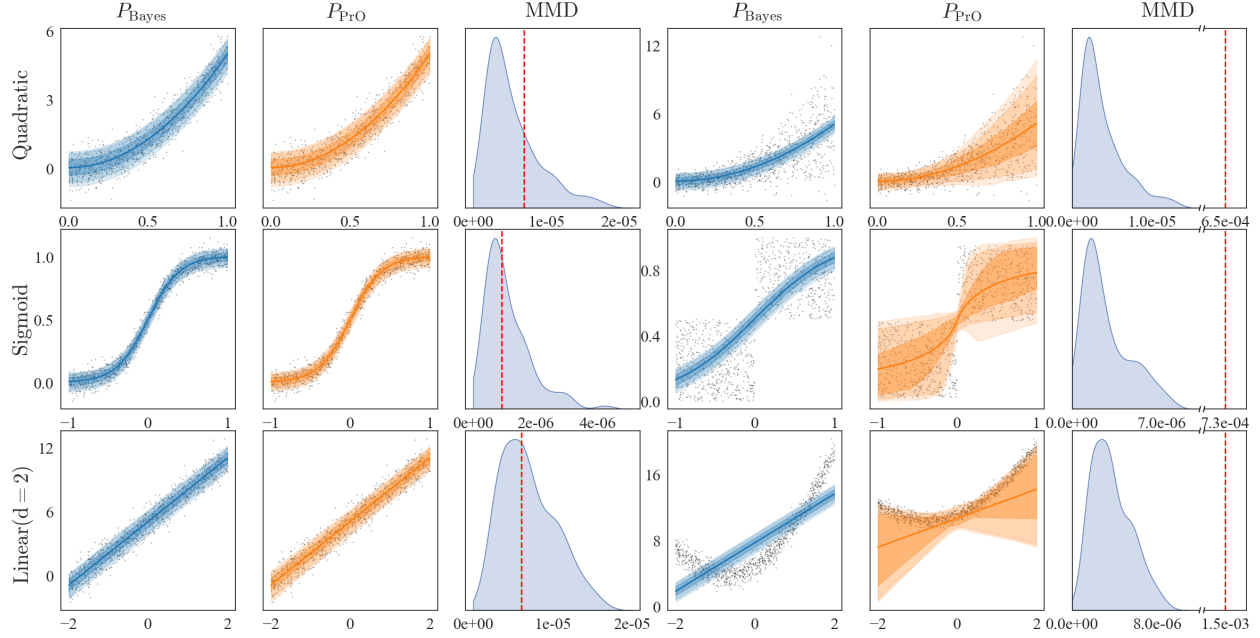


Figure 2: Simulation Study. Each row considers a regression task in which the data are either generated from the statistical model (well-specified, left) or not generated from the statistical model (misspecified, right). The posterior predictive distributions $P_{\text{Bayes}}(\cdot|x)$ (blue) and $P_{\text{PrO}}(\cdot|x)$ (orange) are displayed, along with the null distribution under the hypothesis that the statistical model is well-specified, and the actual realised value of the MMD test statistic D in (10) (red dashed).

3.2 Bayesian Seismic Travel Time Tomography

In seismic travel time tomography, the velocity structure of a medium (e.g., the Earth’s subsurface) is estimated using measured first arrival times of seismic waves propagating between source and receiver locations [Curtis and Snieder, 2002, Zhang and Curtis, 2020, Zhao et al., 2022]. The parameter of interest is a scalar field, with $\theta(x)$ representing wave velocity⁶ at a spatial location $x \in \mathbb{R}^3$. In practice, a bounded domain $\Omega \subset \mathbb{R}^3$ is discretised into a grid and the velocity field θ is represented as a vector of values associated to each cell in the grid, i.e. the velocity is modelled as being piecewise constant. The output of the regression model $f_\theta(x)$ represents the signal received by a seismometer at spatial location x , computed using a physics-constrained simulation using the velocity field θ . Typically, the model $f_\theta(x)$ is governed by the Eikonal equation $|\nabla_x f_\theta(x)| = \theta^{-1}(x)$, a high frequency approximation of the scalar wave equation, and is solved using the fast marching method [Rawlinson and Sambridge, 2005]. The measurement error covariance matrix Σ is assumed to be diagonal Zhao et al. [2022], with diagonal entries σ_i^2 , where σ_i is set equal to 2% of the data associated to the i^{th} channel.

In contrast to the examples in Section 3.1, the need to solve a partial differential equa-

⁶In geophysics it is traditional to refer to speed, i.e. the magnitude of the velocity, simply as *velocity*.

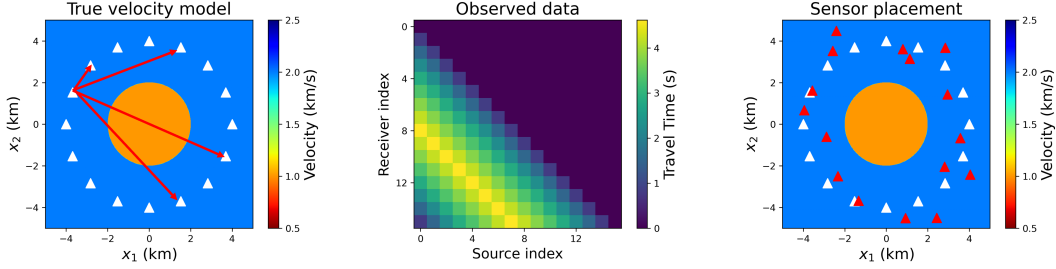


Figure 3: Seismic travel time tomography test-bed. Left: Data are obtained by first emitting a seismic wave from one of the 16 sensors (white triangles) and recording the time at which the wave is detected at each of the other sensors (left panel). Iterating over all sensors results in $n = 256$ travel times, which are noisily observed (centre panel). To simulate a realistic source of model misspecification we consider a setting where the data were generated using the correct sensor placement (white triangles in the right panel) while the statistical model assumes an incorrect sensor placement (red triangles).

tion here to evaluate the statistical model poses a computational barrier to testing for model misspecification based on MMD. As such, here we content ourselves with a qualitative exploration of whether model misspecification can be in principle be detected using Q_{Bayes} and Q_{PrO} in this challenging context. Of course, it is known that the regression model f_θ is to some extent misspecified relative to real world physics. For example, it represents a high frequency approximation of the wave physics, whereas the real case is band-limited. Additionally, travel time tomography relies only on kinematic (phase) information and ignores dynamic (amplitude) information, limiting its ability to reconstruct high resolution velocity structures of the Earth’s interior. However, the key question here is whether the *statistical* model is misspecified in a way that could be scientifically consequential. To assess this, we consider a synthetic test-bed so that we have precise control of exactly how the data are misspecified.

For simplicity, our test-bed is defined for $x \in \mathbb{R}^2$ and is illustrated in the left panel of Figure 3. Here the seismic velocity field θ is piecewise constant, with $\theta(x) = 1$ km/s for $\|z\| \leq 2$, and $\theta(x) = 2$ km/s for $\|z\| > 2$. Data are obtained by first emitting a seismic wave from one of the 16 sensors (depicted by triangles in Figure 3) and recording the time at which the wave is detected at each of the other sensors, as calculated using the fast marching method. Iterating over all 16 sensors yields $n = 256$ readings, each measured with noise governed by the covariance matrix Σ . Since the error model is fixed and known, the measurement error component of the statistical model is always well-specified (see the centre panel of Figure 3). To simulate a realistic source of model misspecification we consider a setting where the data were generated using the correct sensor placement (white triangles in the right panel of Figure 3) while the statistical model assumes an incorrect sensor placement (red triangles). This form of model misspecification is common in earthquake seismological tomography problems, in which the estimation of earthquake source locations can be inaccurate [Dziewonski et al., 1981], affecting the subsequent seismic tomography

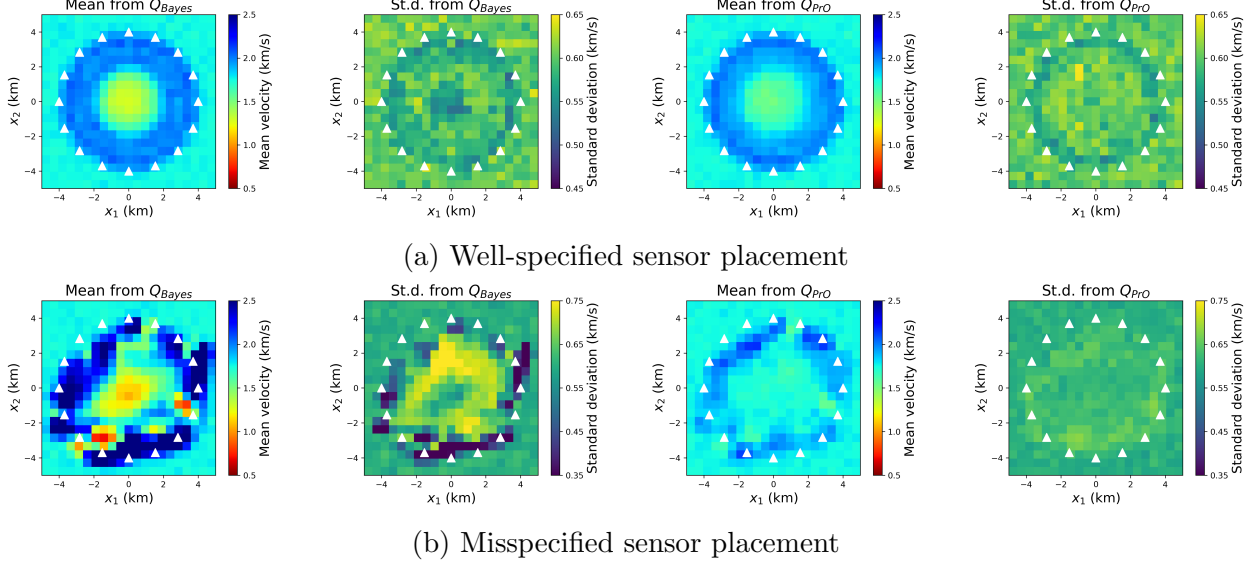


Figure 4: Estimated seismic velocity θ in the setting where the sensor placement assumed in the statistical model is (a) well-specified and (b) misspecified. The standard Bayesian posterior Q_{Bayes} (left) and the predictively oriented posterior Q_{PrO} (right) are almost identical when the statistical model is well-specified, but differ substantially when the statistical model is misspecified.

results.

To facilitate tomographic reconstruction, the spatial domain $\Omega = [-5, 5]^2$ is discretised into a 21×21 grid (the velocity field θ has dimension $d = 441$). The prior distribution Q_0 has each grid cell independent and uniformly distributed over the interval $[0.5, 3]$ km/s; in practice we reparametrised θ from $[0.5, 3]^{21 \times 21}$ to $\mathbb{R}^{21 \times 21}$ to avoid boundary considerations in VGD. Note that the data are non-informative about the region outside the convex hull of the sensors; accordingly the focus is on the reconstruction within the interior of the convex hull. Full details are contained in Section B.5.

Results are shown in Figure 4, where we compare pointwise means and standard deviations for Q_{Bayes} and Q_{PrO} . In the well-specified setting, the distributions Q_{Bayes} and Q_{PrO} appear almost identical. In contrast, under model misspecification, clear differences between Q_{Bayes} and Q_{PrO} can be observed, both in the mean and standard deviation of the reconstructed velocity field. Specifically, Q_{Bayes} is over-confident regarding reconstruction near to the sensors, while such over-confidence is mitigated in Q_{PrO} . (Curiously, Q_{Bayes} also exhibits a *higher* standard deviation than Q_{PrO} for the central region; this indicates to us that reasoning about the impact of model misspecification on Q_{Bayes} is nontrivial.) These results are consistent with the interpretation that comparing Q_{Bayes} and Q_{PrO} can be an effective tool for detecting when a statistical model is misspecified. Indeed, the computational cost of producing the diagnostic plot in Figure 4 is only a factor of 2 larger than the cost of computing Q_{Bayes} itself.

4 Discussion

As statisticians we seek to avoid making predictions which are simultaneously highly confident and incorrect, but this scenario occurs generically in Bayesian analyses when the data are informative and the statistical model is misspecified. To address this challenge, we combined the emerging ideas of predictively oriented inference and variational gradient descent to obtain a simple, practical and general approach to detect model misspecification in the Bayesian context. An appealing aspect of our approach is that we do not require data splitting (e.g. as in posterior predictive checks) or the manual specification of alternative statistical models (as in comparative approaches). The approach was successfully demonstrated both in simulation studies and in the challenging seismic travel time tomography context.

Our focus was limited to statistical and computational methodology; although we indicated how one could formulate a formal hypothesis test, we did not attempt to establish asymptotic correctness of this test. This theoretical analysis would be an interesting topic for future work [e.g. extending Key et al., 2021, to the case of data that are conditionally independent].

In settings where our diagnostic indicates possible model misspecification, an obvious next question is *how to proceed with a misspecified model?* This important question is outside the scope of the present work, but has been the subject of considerable research effort. Potential solutions include nonparametric learning of the correct model [Kennedy and O’Hagan, 2001, Alvarez et al., 2013] and judicious use of an incorrect model [Bissiri et al., 2016, Knoblauch et al., 2022]; a recent review is provided by Nott et al. [2023]. An interesting emerging alternative is to use the predictively oriented ‘posterior’ in place of the standard Bayesian posterior [Masegosa, 2020, Sheth and Khardon, 2020, Jankowiak et al., 2020a,b, Morningstar et al., 2022, Lai and Yao, 2024, Shen et al., 2025, McLatchie et al., 2025].

Acknowledgments QL was supported by the China Scholarship Council 202408060123. CJO, ZS were supported by EPSRC EP/W019590/1. CJO was supported by a Philip Leverhulme Prize PLP-2023-004. XZ and AC thank the Edinburgh Imaging Project (EIP) sponsors (BP and TotalEnergies) for supporting this research. The authors are grateful to François-Xavier Briol, Badr-Eddine Chérif-Abdellatif, David Frazier, Jeremias Knoblauch and Yann McLatchie for insightful discussion during the completion of this work.

References

- M. A. Alvarez, D. Luengo, and N. D. Lawrence. Linear latent force models using Gaussian processes. *IEEE Transactions on Pattern Analysis and Machine Intelligence*, 35(11):2693–2705, 2013.
- L. Ambrosio, N. Gigli, and G. Savaré. *Gradient Flows: In Metric Spaces and in the Space of Probability Measures*. Springer Science & Business Media, 2008.

- S. Banerjee, K. Balasubramanian, and P. Ghosal. Improved finite-particle convergence rates for Stein variational gradient descent. In *The Thirteenth International Conference on Learning Representations*, 2025.
- M. Bayarri and J. O. Berger. P values for composite null models. *Journal of the American Statistical Association*, 95(452):1127–1142, 2000.
- P. G. Bissiri, C. C. Holmes, and S. G. Walker. A general framework for updating belief distributions. *Journal of the Royal Statistical Society Series B: Statistical Methodology*, 78(5):1103–1130, 2016.
- P. Burman, E. Chow, and D. Nolan. A cross-validatory method for dependent data. *Biometrika*, 81(2):351–358, 1994.
- C. Chazal, H. Kanagawa, Z. Shen, A. Korba, and C. J. Oates. A computable measure of suboptimality for entropy-regularised variational objectives. *arXiv preprint*, 2025.
- A. Curtis and R. Snieder. Probing the earth’s interior with seismic tomography. *International Geophysics*, 81A:861–874, 2002.
- P. Del Moral. Mean field simulation for Monte Carlo integration. *Monographs on Statistics and Applied Probability*, 126(26):6, 2013.
- P. Dupuis and R. S. Ellis. *A Weak Convergence Approach to the Theory of Large Deviations*. John Wiley & Sons, 2011.
- A. M. Dziewonski, T.-A. Chou, and J. H. Woodhouse. Determination of earthquake source parameters from waveform data for studies of global and regional seismicity. *Journal of Geophysical Research: Solid Earth*, 86(B4):2825–2852, 1981.
- E. Fong and C. C. Holmes. On the marginal likelihood and cross-validation. *Biometrika*, 107(2):489–496, 2020.
- D. Garreau, W. Jitkrittum, and M. Kanagawa. Large sample analysis of the median heuristic. *arXiv preprint arXiv:1707.07269*, 2017.
- A. Gelman, X.-L. Meng, and H. Stern. Posterior predictive assessment of model fitness via realized discrepancies. *Statistica Sinica*, 6(4):733–760, 1996.
- P. Hartman. *Ordinary Differential Equations*. SIAM, 2002.
- K. Hu, Z. Ren, D. Šiška, and L. Szpruch. Mean-field Langevin dynamics and energy landscape of neural networks. *Annales de l’Institut Henri Poincaré (B) Probabilités et statistiques*, 57(4):2043–2065, 2021.
- M. Jankowiak, G. Pleiss, and J. Gardner. Deep sigma point processes. In *Conference on Uncertainty in Artificial Intelligence*, pages 789–798. PMLR, 2020a.

- M. Jankowiak, G. Pleiss, and J. Gardner. Parametric Gaussian process regressors. In *International Conference on Machine Learning*, pages 4702–4712. PMLR, 2020b.
- K. Kamary, K. Mengersen, C. P. Robert, and J. Rousseau. Testing hypotheses via a mixture estimation model. *arXiv preprint arXiv:1412.2044*, 2014.
- R. E. Kass and A. E. Raftery. Bayes factors. *Journal of the American Statistical Association*, 90(430):773–795, 1995.
- M. C. Kennedy and A. O’Hagan. Bayesian calibration of computer models. *Journal of the Royal Statistical Society Series B*, 63(3):425–464, 2001.
- O. Key, A. Gretton, F.-X. Briol, and T. Fernandez. Composite goodness-of-fit tests with kernels. *arXiv preprint arXiv:2111.10275*, 2021.
- J. Knoblauch, J. Jewson, and T. Damoulas. An optimization-centric view on Bayes’ rule: Reviewing and generalizing variational inference. *Journal of Machine Learning Research*, 23(132):1–109, 2022.
- J. Lai and Y. Yao. Predictive variational inference: Learn the predictively optimal posterior distribution. *arXiv preprint arXiv:2410.14843*, 2024.
- N. Laird. Nonparametric maximum likelihood estimation of a mixing distribution. *Journal of the American Statistical Association*, 73(364):805–811, 1978.
- B. G. Lindsay. *Mixture Models: Theory, Geometry, and Applications*. 1995.
- Q. Liu and D. Wang. Stein variational gradient descent: A general purpose Bayesian inference algorithm. *Advances in Neural Information Processing Systems*, (30):2378–2386, 2016.
- A. Masegosa. Learning under model misspecification: Applications to variational and ensemble methods. *Advances in Neural Information Processing Systems*, 33:5479–5491, 2020.
- Y. McLatchie, B.-E. Cherief-Abdellatif, D. T. Frazier, and J. Knoblauch. Predictively oriented posteriors. *arXiv preprint arXiv:2510.01915*, 2025.
- G. E. Moran, D. M. Blei, and R. Ranganath. Holdout predictive checks for Bayesian model criticism. *Journal of the Royal Statistical Society Series B*, 86(1):194–214, 2024.
- W. R. Morningstar, A. Alemi, and J. V. Dillon. PACm-Bayes: Narrowing the empirical risk gap in the misspecified Bayesian regime. In *International Conference on Artificial Intelligence and Statistics*, pages 8270–8298. PMLR, 2022.
- D. J. Nott, C. Drovandi, and D. T. Frazier. Bayesian inference for misspecified generative models. *Annual Review of Statistics and Its Application*, 11:179–202, 2023.
- J. Piironen and A. Vehtari. Comparison of Bayesian predictive methods for model selection. *Statistics and Computing*, 27(3):711–735, 2017.

- A. Rabinowicz and S. Rosset. Cross-validation for correlated data. *Journal of the American Statistical Association*, 117(538):718–731, 2022.
- N. Rawlinson and M. Sambridge. The fast marching method: An effective tool for tomographic imaging and tracking multiple phases in complex layered media. *Exploration Geophysics*, 36(4):341–350, 2005.
- D. B. Rubin. Bayesianly justifiable and relevant frequency calculations for the applied statistician. *The Annals of Statistics*, 12(4):1151–1172, 1984.
- Z. Shen, J. Knoblauch, S. Power, and C. J. Oates. Prediction-centric uncertainty quantification via MMD. In *AISTATS*, 2025.
- R. Sheth and R. Kharon. Pseudo-Bayesian learning via direct loss minimization with applications to sparse Gaussian process models. In *Symposium on Advances in Approximate Bayesian Inference*, pages 1–18. PMLR, 2020.
- S. G. Walker. Bayesian inference with misspecified models. *Journal of Statistical Planning and Inference*, 143(10):1621–1633, 2013.
- D. Wang and Q. Liu. Nonlinear Stein variational gradient descent for learning diversified mixture models. In *International Conference on Machine Learning*, pages 6576–6585. PMLR, 2019.
- L. Wasserman. Bayesian model selection and model averaging. *Journal of Mathematical Psychology*, 44(1):92–107, 2000.
- P.-S. Wu and R. Martin. A comparison of learning rate selection methods in generalized Bayesian inference. *Bayesian Analysis*, 18(1):105–132, 2023.
- A. Zellner. Optimal information processing and Bayes’s theorem. *The American Statistician*, 42(4):278–280, 1988.
- X. Zhang and A. Curtis. Seismic tomography using variational inference methods. *Journal of Geophysical Research: Solid Earth*, 125(4):e2019JB018589, 2020.
- X. Zhang, A. Lomas, M. Zhou, Y. Zheng, and A. Curtis. 3-D Bayesian variational full waveform inversion. *Geophysical Journal International*, 234(1):546–561, 2023.
- X. Zhao, A. Curtis, and X. Zhang. Bayesian seismic tomography using normalizing flows. *Geophysical Journal International*, 228(1):213–239, 2022.

A Proofs

This appendix contains proofs for all theoretical results in the main text. Preliminary results are contained in Section A.1, while Proposition 1 is proven in Section A.2, Proposition 2 is proven in Section A.3, and Proposition 3 is proven in Section A.4.

Additional Notation Let $b_Q(\theta) := (\nabla \log q_0)(\theta) - \nabla_V \mathcal{L}(Q)(\theta)$ for all $Q \in \mathcal{P}(\mathbb{R}^d)$ and all $\theta \in \mathbb{R}^d$. This can be considered a Q -dependent generalisation of the *Stein score* [Liu and Wang, 2016], which is recovered in the case of linear \mathcal{L} . For $f, g : \mathbb{R}^d \rightarrow \mathbb{R}$, write $f(x) \lesssim g(x)$ if there exists a finite constant C such that $f(x) \leq Cg(x)$ for all $x \in \mathbb{R}^d$. For a suitably differentiable function f , let $\nabla^2 f$ denote the matrix of mixed partial derivatives $\partial_i \partial_j f$.

A.1 Preliminary Results

First we derive the variational gradient of \mathcal{L}_{PrO} :

Proposition 4 (Explicit form of variational gradient). *Let $\mathcal{L} = \mathcal{L}_{\text{PrO}}$. Let $\theta \mapsto p_\theta(y_i|x_i)$ be positive, bounded and differentiable for each (x_i, y_i) in the dataset. Then*

$$\nabla_V \mathcal{L}(Q)(\theta) = - \sum_{i=1}^n \frac{\nabla_\theta p_\theta(y_i|x_i)}{p_Q(y_i|x_i)}. \quad (12)$$

Proof. The first variation is

$$\mathcal{L}'(Q)(\theta) = - \sum_{i=1}^n \frac{p_\theta(y_i|x_i)}{p_Q(y_i|x_i)} \quad (13)$$

which is well-defined since, under our assumptions, $p_Q(y_i|x_i) = \int p_\theta(y_i|x_i) dQ(\theta)$ is strictly positive (so the denominator in (13) is non-zero) and bounded (so (13) is integrable with respect to all perturbations $\chi \in \mathcal{P}(\mathbb{R}^d)$; cf. the definition of first variation in Section 2.2) for all $Q \in \mathcal{P}(\mathbb{R}^d)$ and all (x_i, y_i) in the dataset. The variational gradient is thus (12), where the derivatives were assumed to be well-defined. \square

The following specialises Proposition 1 in Chazal et al., 2025, which deals with general matrix-values kernels $K(\theta, \vartheta)$ to the case of a scalar kernel, i.e. $K(\theta, \vartheta) = k(\theta, \vartheta)I_{d \times d}$, and presents an explicit formula for the KGD.

Proposition 5 (Computable form of KGD; special case of Proposition 1 in Chazal et al., 2025). *Let Q_0 have a density $q_0 > 0$ on \mathbb{R}^d . Let b_Q be well-defined. Let k be a symmetric positive semi-definite kernel for which $\nabla_1 k$ and $\nabla_1 \cdot \nabla_2 k$ are well-defined. Suppose $\mathcal{T}_Q \mathcal{H}_k^d \subset \mathcal{L}^1(Q)$. Then*

$$\text{KGD}_k(Q) = \left(\iint k_Q(\theta, \vartheta) dQ(\theta) dQ(\vartheta) \right)^{1/2}$$

where

$$k_Q(\theta, \vartheta) := \nabla_1 \cdot \nabla_2 k(\theta, \vartheta) + \nabla_1 k(\theta, \vartheta) \cdot b_Q(\vartheta) + \nabla_2 k(\theta, \vartheta) \cdot b_Q(\theta) + k(\theta, \vartheta) b_Q(\theta) \cdot b_Q(\vartheta)$$

is a Q -dependent kernel.

In particular, for $Q_n = \frac{1}{n} \sum_{i=1}^n \delta_{\theta_i}$ an empirical distribution,

$$\text{KGD}_k^2(Q) = \frac{1}{n^2} \sum_{i=1}^n \sum_{j=1}^n \left\{ \begin{aligned} &\nabla_1 \cdot \nabla_2 k(\theta_i, \theta_j) + \nabla_1 k(\theta_i, \theta_j) \cdot b_Q(\theta_j) \\ &+ \nabla_2 k(\theta_i, \theta_j) \cdot b_Q(\theta_i) + k(\theta_i, \theta_j) b_Q(\theta_i) \cdot b_Q(\theta_j) \end{aligned} \right\} \quad (14)$$

which allows for KGD to be explicitly computed.

A.2 Proof of Proposition 1

Proof of Proposition 1. Introduce the shorthand

$$\mathcal{J}(Q) = \mathcal{L}(Q) + \text{KLD}(Q||Q_0), \quad \mathcal{L}(Q) = \mathcal{L}_{\text{PrO}}(Q) = - \sum_{i=1}^n \log p_Q(y_i|x_i).$$

Under our assumptions \mathcal{L} is weakly continuous, since if $Q_n \rightarrow Q$ weakly then

$$\int p_\theta(y_i|x_i) \, dQ_n(\theta) \rightarrow \int p_\theta(y_i|x_i) \, dQ(\theta)$$

since the integrand is bounded. Thus

$$\mathcal{L}(Q_n) = - \sum_{i=1}^n \log \int p_\theta(y_i|x_i) \, dQ_n(\theta) \rightarrow - \sum_{i=1}^n \log \int p_\theta(y_i|x_i) \, dQ(\theta) = \mathcal{L}(Q),$$

as claimed. Further note that \mathcal{L} is convex, since for $Q, Q' \in \mathcal{P}(\mathbb{R}^d)$ and $t \in (0, 1)$,

$$\begin{aligned} \mathcal{L}(tQ + (1-t)Q') &= - \sum_{i=1}^n \log \left[t \int p_\theta(y_i|x_i) \, dQ(\theta) + (1-t) \int p_\theta(y_i|x_i) \, dQ'(\theta) \right] \\ &\leq -t \sum_{i=1}^n \log \int p_\theta(y_i|x_i) \, dQ(\theta) - (1-t) \sum_{i=1}^n \log \int p_\theta(y_i|x_i) \, dQ'(\theta) \\ &= t\mathcal{L}(Q) + (1-t)\mathcal{L}(Q') \end{aligned}$$

by convexity of $z \mapsto -\log(z)$. Since $\text{KLD}(\cdot||Q_0)$ is weakly lower semi-continuous and strictly convex, it follows that \mathcal{J} is as well. The rest of the proof follows a standard argument [e.g. Proposition 5 in Hu et al., 2021]. To this end, note that

$$\mathcal{S} := \left\{ Q \in \mathcal{P}(\mathbb{R}^d) : \text{KLD}(Q||Q_0) \leq \mathcal{J}(Q_0) - \inf_{Q \in \mathcal{P}(\mathbb{R}^d)} \mathcal{L}(Q') \right\}.$$

is a (non-empty, since $Q_0 \in \mathcal{S}$) sub-level set of the KLD and is therefore weakly compact [Dupuis and Ellis, 2011, Lemma 1.4.3]. Since \mathcal{J} is weakly lower semi-continuous, the minimum of \mathcal{J} on \mathcal{S} is attained. Since $\mathcal{J}(Q) \geq \mathcal{J}(Q_0)$ for all $Q \notin \mathcal{S}$, the minimum of \mathcal{J} on \mathcal{S} coincides with the global minimum of \mathcal{J} . Since \mathcal{J} is strictly convex, the minimum is unique. The final claim is the content of Proposition 6. \square

Proposition 6 (Moments for Q_{PrO}). *Assume that $Q_0 \in \mathcal{P}_\alpha(\mathbb{R}^d)$ admits a positive and bounded density q_0 on \mathbb{R}^d . Let $\theta \mapsto p_\theta(y_i|x_i)$ be bounded for each (x_i, y_i) in the dataset. Then $Q_{\text{PrO}} \in \mathcal{P}_\alpha(\mathbb{R}^d)$.*

Proof. Following the same argument used to prove Proposition 4, the first variation $\mathcal{L}'_{\text{PrO}}$ is well-defined. Since Q_{PrO} is the minimiser of \mathcal{J} , following Chazal et al. [2025, Corollary 2] it is also a solution of the stationary point equation

$$\text{cst} = \mathcal{L}'_{\text{PrO}}(Q) + 1 + \log \frac{dQ}{dQ_0}$$

which implies Q_{PrO} has a density $q_{\text{PrO}}(\theta) \propto \exp(-\mathcal{L}'_{\text{PrO}}(Q_{\text{PrO}})(\theta))q_0(\theta)$ on \mathbb{R}^d . From (13) and our assumption, $\mathcal{L}'_{\text{PrO}}(Q_{\text{PrO}})$ is bounded. The conclusion therefore follows from the assumption $Q_0 \in \mathcal{P}_\alpha(\mathbb{R}^d)$. \square

A.3 Proof of Proposition 2

The main idea behind the proof of Proposition 2 is to undertake a refinement of the analysis of VGD in Chazal et al. [2025]; we do this in Section A.3.1. Then we verify that our refined regularity conditions hold in Section A.3.2, enabling the proof of Proposition 2 to be presented in Section A.3.3.

A.3.1 Refined Analysis of VGD

The following result relaxes the conditions of Proposition 3 in Chazal et al. [2025], to obtain a result that is applicable in our context; further details can be found in Remark 4. Note that Proposition 3 in Chazal et al. [2025] is in turn a generalisation (to VGD) of the analysis of SVGD presented in Theorem 1 of Banerjee et al. [2025].

For a sufficiently regular $\mathcal{F} : \mathcal{P}(\mathbb{R}^d) \rightarrow \mathbb{R}$, let $\nabla_V \cdot \nabla_V \mathcal{F}(Q)$ denote the function $(x, y) \mapsto \sum_i \partial_i \mathcal{G}'_{x,i}(Q)(y)$ where $\mathcal{G}_x(Q) := \nabla_V \mathcal{F}(Q)(x)$.

Theorem 1 (Refined analysis of VGD). *Assume that:*

1. (Integrability) $\exp(-\mathcal{L}'(Q)) \in \mathcal{L}^1(Q_0)$ for all $Q \in \mathcal{P}(\mathbb{R}^d)$
2. (Loss) the map $(\theta_1, \dots, \theta_N) \mapsto \nabla_V \mathcal{L}(Q_N)(\theta_j)$ is $C^2(\mathbb{R}^{d \times N})$ for each $j \in \{1, \dots, N\}$, with
 - a. $\sup_{Q \in \mathcal{P}(\mathbb{R}^d)} \left| \int k(\theta, \theta) \nabla \cdot \nabla_V \mathcal{L}(Q)(\theta) dQ(\theta) \right| < \infty$,
 - b. $\sup_{Q \in \mathcal{P}(\mathbb{R}^d)} \left| \iint k(\theta, \vartheta) \nabla_V \cdot \nabla_V \mathcal{L}(Q)(\theta)(\vartheta) dQ(\theta) dQ(\vartheta) \right| < \infty$
3. (Regularisation) $\log q_0 \in C^3(\mathbb{R}^d)$ with $\sup_{\theta \in \mathbb{R}^d} k(\theta, \theta) |\Delta \log q_0(\theta)| < \infty$.
4. (Initialisation) μ_0 has bounded support, and has a density that is $C^2(\mathbb{R}^d)$.
5. (Kernel) k is $C^3(\mathbb{R}^d)$ in each argument with $\sup_{\theta \in \mathbb{R}^d} |\Delta_1 k(\theta, \theta)| < \infty$.
6. (Growth) the maps $(\theta_1, \dots, \theta_N) \mapsto k(\theta_j, \theta_j) \|\nabla \log q_0(\theta_j)\|$, $k(\theta_j, \theta_j) \|\nabla_V \mathcal{L}(Q_N)(\theta_j)\|$ and $\|\nabla_1 k(\theta_j, \theta_i)\|$ have at most linear growth for each $\{i, j\} \in \{1, \dots, N\}$.

Then the dynamics defined in (8) satisfies

$$\frac{1}{T} \int_0^T \mathbb{E}[\text{KGD}_k^2(Q_N^t)] dt \leq \frac{\text{KLD}(\mu_0 \parallel \rho_{\mu_0})}{T} + \frac{C_k}{N}$$

for some finite constant C_k , where ρ_{μ_0} denotes the distribution with density proportional to $q_0(\theta) \exp(-\mathcal{L}'(\mu_0)(\theta))$.

Proof. The proof is organised into four steps:

Step 1: Existence of a joint density with bounded support. Introduce the shorthand $\boldsymbol{\theta} := (\theta_1, \dots, \theta_N) \in \mathbb{R}^{d \times N}$ and

$$\Phi_{\boldsymbol{\theta}}(\theta_i, \theta_j) := k(\theta_i, \theta_j) \underbrace{(\nabla \log q_0 - \nabla_{\mathbf{V}} \mathcal{L}(Q_N))(\theta_j)}_{=: b_{Q_N}(\theta_j)} + \nabla_1 k(\theta_j, \theta_i), \quad Q_N := \frac{1}{N} \sum_{j=1}^N \delta_{\theta_j},$$

where for convenience we have suppressed the t -dependence, i.e. $\theta_i \equiv \theta_i(t)$ and $Q_N \equiv Q_N(\boldsymbol{\theta})$. Under our assumptions, $\boldsymbol{\theta} \mapsto \Phi_{\boldsymbol{\theta}}(\theta_i, \theta_j)$ is $C^2(\mathbb{R}^{d \times N})$. Further, from Item 6, $\Phi_{\boldsymbol{\theta}}(\theta_i, \theta_j)$ has at most linear growth as a function of $\boldsymbol{\theta}$; i.e. $|\Phi_{\boldsymbol{\theta}}(\theta_i, \theta_j)| \lesssim 1 + \|\boldsymbol{\theta}\|$.

Since $\boldsymbol{\theta} \mapsto \Phi_{\boldsymbol{\theta}}(\theta_i, \theta_j)$ is $C^2(\mathbb{R}^{d \times N})$, from Hartman [2002, Chapter 5, Cor. 4.1] there exists a joint density $p_N(t, \cdot)$ for $\boldsymbol{\theta}(t)$ for all $t \in [0, \infty)$ and, following an analogous argument to Lemma 1 in Banerjee et al. [2025], $(t, \boldsymbol{\theta}) \mapsto p_N(t, \boldsymbol{\theta})$ is $C^2([0, \infty) \times \mathbb{R}^{d \times N})$. This mapping $p_N(t, \cdot)$ is a solution of the N -body Liouville equation

$$\partial_t p_N(t, \boldsymbol{\theta}) + \frac{1}{N} \sum_{i=1}^N \sum_{j=1}^N \nabla_{\theta_i} \cdot (p_N(t, \boldsymbol{\theta}) \Phi_{\boldsymbol{\theta}}(\theta_i, \theta_j)) = 0, \quad (15)$$

see Ambrosio et al. [2008, Chapter 8]. Further, since $p_N(0, \cdot) = \mu_0(\cdot)$ has bounded support and the drift $\boldsymbol{\theta} \mapsto \Phi_{\boldsymbol{\theta}}(\theta_i, \theta_j)$ has at most linear growth, each $p_N(t, \cdot)$ also has bounded support.

Step 2: Descent on the KLD. From Item 1, the distribution ρ_Q with density proportional to $q_0(\theta) \exp(-\mathcal{L}'(Q)(\theta))$ is well-defined.

Let $H(t) := \text{KLD}(p_N(t, \cdot) \| \rho_{Q_N}^{\otimes N})$ so that, using (15),

$$\begin{aligned} H'(t) &= \partial_t \int \log \left(\frac{p_N(t, \boldsymbol{\theta})}{\rho_{Q_N}(\theta_1) \cdots \rho_{Q_N}(\theta_N)} \right) p_N(t, \boldsymbol{\theta}) \, d\boldsymbol{\theta} \\ &= \underbrace{\int \partial_t p_N(t, \boldsymbol{\theta}) \, d\boldsymbol{\theta}}_{=0} + \int \log \left(\frac{p_N(t, \boldsymbol{\theta})}{\rho_{Q_N}(\theta_1) \cdots \rho_{Q_N}(\theta_N)} \right) \partial_t p_N(t, \boldsymbol{\theta}) \, d\boldsymbol{\theta} \\ &= - \int \frac{1}{N} \sum_{i=1}^N \sum_{j=1}^N \log \left(\frac{p_N(t, \boldsymbol{\theta})}{\rho_{Q_N}(\theta_1) \cdots \rho_{Q_N}(\theta_N)} \right) \nabla_{\theta_i} \cdot (p_N(t, \boldsymbol{\theta}) \Phi_{\boldsymbol{\theta}}(\theta_i, \theta_j)) \, d\boldsymbol{\theta}. \end{aligned}$$

The interchanges of ∂_t and integrals are justified by the dominated convergence theorem and noting that all integrands are $C^2([0, \infty) \times \mathbb{R}^{d \times N})$ and vanish when $\boldsymbol{\theta}$ lies outside of a bounded subset of $\mathbb{R}^{d \times N}$ (i.e. uniformly over $t \in [0, T]$). Then, noting that $v : \mathbb{R}^{d \times N} \rightarrow \mathbb{R}^{d \times N}$ with $v = (v_1, \dots, v_N)$ and

$$v_i(\boldsymbol{\theta}) := \log \left(\frac{p_N(t, \boldsymbol{\theta})}{\rho_{Q_N}(\theta_1) \cdots \rho_{Q_N}(\theta_N)} \right) p_N(t, \boldsymbol{\theta}) \Phi_{\boldsymbol{\theta}}(\theta_i, \theta_j),$$

is $C^1(\mathbb{R}^{d \times N})$ and vanishes outside of a bounded set, and is therefore $\mathcal{L}^1(\mathbb{R}^{d \times N})$, we may use integration-by-parts [e.g. Chazal et al., 2025, Lemma 1]:

$$\begin{aligned} H'(t) &= \frac{1}{N} \sum_{i=1}^N \sum_{j=1}^N \int \nabla_{\theta_i} \log \left(\frac{p_N(t, \boldsymbol{\theta})}{\rho_{Q_N}(\theta_1) \cdots \rho_{Q_N}(\theta_N)} \right) \cdot (p_N(t, \boldsymbol{\theta}) \Phi_{\boldsymbol{\theta}}(\theta_i, \theta_j)) \, d\boldsymbol{\theta} \\ &= \frac{1}{N} \sum_{i=1}^N \sum_{j=1}^N \int \nabla_{\theta_i} p_N(t, \boldsymbol{\theta}) \cdot \Phi_t(\theta_i, \theta_j) - b_{Q_N}(\theta_i) \cdot \Phi_{\boldsymbol{\theta}}(\theta_i, \theta_j) p_N(t, \boldsymbol{\theta}) \, d\boldsymbol{\theta} \end{aligned}$$

Similarly noting that $\boldsymbol{\theta} \mapsto p_N(t, \boldsymbol{\theta}) \Phi_{\boldsymbol{\theta}}(\theta_i, \theta_j)$ is $\mathcal{L}^1(\mathbb{R}^{d \times N})$, another application of integration-by-parts yields

$$\begin{aligned} H'(t) &= -\frac{1}{N} \sum_{i=1}^N \sum_{j=1}^N \int (\nabla_{\theta_i} \cdot \Phi_t(\theta_i, \theta_j) + b_{Q_N}(\theta_i) \cdot \Phi_{\boldsymbol{\theta}}(\theta_i, \theta_j)) p_N(t, \boldsymbol{\theta}) \, d\boldsymbol{\theta} \\ &= -\mathbb{E} \left[\frac{1}{N} \sum_{i=1}^N \sum_{j=1}^N \nabla_{\theta_i} \cdot \Phi_t(\theta_i, \theta_j) + b_{Q_N}(\theta_i) \cdot \Phi_{\boldsymbol{\theta}}(\theta_i, \theta_j) \right] \end{aligned} \quad (16)$$

where we have used the expectation shorthand to refer to the random initialisation of the particles.

Step 3: Calculating derivatives. Now we aim to calculate the terms in (16). Since k is a differentiable kernel we have $\nabla_1 k(\theta, \theta) = 0$ for all $\theta \in \mathbb{R}^d$, and

$$\begin{aligned} \nabla_{\theta_i} \cdot \Phi_{\boldsymbol{\theta}}(\theta_i, \theta_j) &= \nabla_{\theta_i} \cdot [k(\theta_i, \theta_j) b_{Q_N}(\theta_j)] + \nabla_{\theta_i} \cdot [\nabla_1 k(\theta_j, \theta_i)] \\ &= \nabla_1 k(\theta_i, \theta_j) \cdot b_{Q_N}(\theta_j) + k(\theta_i, \theta_j) \nabla_{\theta_i} \cdot b_{Q_N}(\theta_j) + \nabla_1 \cdot \nabla_2 k(\theta_i, \theta_j) \\ &\quad + \underbrace{\{\nabla_1 k(\theta_i, \theta_i) \cdot b_{Q_N}(\theta_i) + \Delta_1 k(\theta_i, \theta_i)\}}_{=0} \mathbb{1}_{i=j} \\ b_{Q_N}(\theta_i) \cdot \Phi_{\boldsymbol{\theta}}(\theta_i, \theta_j) &= k(\theta_i, \theta_j) b_{Q_N}(\theta_i) \cdot b_{Q_N}(\theta_j) + b_{Q_N}(\theta_i) \cdot \nabla_1 k(\theta_j, \theta_i) \end{aligned}$$

and

$$\nabla_{\theta_i} \cdot b_{Q_N}(\theta_j) = \{\nabla \cdot (\nabla \log q_0 - \nabla_V \mathcal{L}(Q_N))(\theta_i)\} \mathbb{1}_{i=j} - \frac{1}{n} \nabla_V \cdot \nabla_V \mathcal{L}(Q_N)(\theta_j)(\theta_i).$$

Thus, collecting together terms that correspond to KGD using (14),

$$\begin{aligned} H'(t) &= -N \mathbb{E} \left[\text{KGD}_k^2(Q_N) - \frac{1}{N^2} \sum_{i=1}^N \sum_{j=1}^N k(\theta_i, \theta_j) \nabla_V \cdot \nabla_V \mathcal{L}(Q_N)(\theta_j)(\theta_i) \right. \\ &\quad \left. - \frac{1}{N^2} \sum_{i=1}^N k(\theta_i, \theta_i) [\Delta \log q_0(\theta_i) - \nabla \cdot \nabla_V \mathcal{L}(Q_N)(\theta_i)] + \Delta_1 k(\theta_i, \theta_i) \right]. \end{aligned} \quad (17)$$

Step 4: Obtaining a bound. The final task is to bound the non-KGD terms appearing in (17) by a Q_N -independent constant. Under our assumptions,

$$\begin{aligned}
& \left| \frac{1}{N^2} \sum_{i=1}^N \sum_{j=1}^N k(\theta_i, \theta_j) \nabla_V \cdot \nabla_V \mathcal{L}(Q_N)(\theta_j)(\theta_i) \right| \\
& \leq \sup_{Q \in \mathcal{P}(\mathbb{R}^d)} \left| \iint k(\theta, \vartheta) \nabla_V \cdot \nabla_V \mathcal{L}(Q)(\theta)(\vartheta) \, dQ(\theta) dQ(\vartheta) \right| < \infty \\
& \left| \frac{1}{N^2} \sum_{i=1}^N k(\theta_i, \theta_i) [\Delta \log q_0(\theta_i) - \nabla \cdot \nabla_V \mathcal{L}(Q_N)(\theta_i)] + \Delta_1 k(\theta_i, \theta_i) \right| \\
& \leq \sup_{\theta \in \mathbb{R}^d} k(\theta, \theta) |\Delta \log q_0(\theta)| \\
& \quad + \sup_{Q \in \mathcal{P}(\mathbb{R}^d)} \left| \int k(\theta, \theta) \nabla \cdot \nabla_V \mathcal{L}(Q)(\theta) \, dQ(\theta) \right| + \sup_{\theta \in \mathbb{R}^d} \Delta_1 k(\theta, \theta) < \infty
\end{aligned}$$

which establish the required bounds, i.e.

$$H'(t) \leq -N\mathbb{E}[\text{KGD}_k^2(Q_N)] + C_k$$

for some finite, k -dependent constant C_k . Integrating both sides from 0 to T and rearranging yields

$$\frac{1}{T} \int_0^T \mathbb{E}[\text{KGD}_k^2(Q_N)] \, dt \leq \frac{H(0) - H(t)}{NT} + \frac{C_k}{N} \leq \frac{H(0)}{NT} + \frac{C_k}{N}.$$

The result follows from additivity of the KLD, since $H(0) = N\text{KLD}(\mu_0 || \rho_{\mu_0})$. \square

Remark 4 (Relaxing the conditions of Proposition 3 in Chazal et al. [2025]). *Compared to Proposition 3 in Chazal et al. [2025] we have relaxed both Item 2 on the loss and condition Item 5 on the kernel. In Item 2 we have relaxed boundedness conditions on $\nabla \nabla_V \mathcal{L}$ and $\nabla_V \cdot \nabla_V \mathcal{L}$ (which do not hold for \mathcal{L}_{mix} in our context) into integrability conditions on $\nabla \cdot \nabla_V \mathcal{L}$ and $\nabla_V \cdot \nabla_V \mathcal{L}$ (which, as we will see, do hold under appropriate assumptions on P_θ). In condition Item 5 we have also relaxed the assumption that the kernel is translation-invariant.*

A.3.2 Verifying Regularity Conditions

Theorem 1 applied to general loss functions \mathcal{L} ; here we establish explicit sufficient conditions in the specific case of \mathcal{L}_{PRO} .

Proposition 7 (Regularity for the variational gradient of \mathcal{L}_{PRO}). *Let $p_\theta(y_i|x_i)$ be a positive density for all $\theta \in \mathbb{R}^d$ and each (x_i, y_i) in the dataset. Let*

1. $\sup_{\theta \in \mathbb{R}^d} p_\theta(y_i|x_i) < \infty$
2. $\sup_{\theta \in \mathbb{R}^d} \sqrt{k(\theta, \theta)} \frac{\|\nabla_\theta p_\theta(y_i|x_i)\|}{p_\theta(y_i|x_i)} < \infty$

$$3. \sup_{\theta \in \mathbb{R}^d} k(\theta, \theta) \frac{\Delta_\theta p_\theta(y_i|x_i)}{p_\theta(y_i|x_i)} < \infty$$

for each (x_i, y_i) in the dataset. Then the map $\theta \mapsto k(\theta, \theta) \|\nabla_\theta p_\theta(y_i|x_i)\|$ has at most linear growth and, for the loss function $\mathcal{L} = \mathcal{L}_{\text{PrO}}$ in (3),

$$\sup_{Q \in \mathcal{P}(\mathbb{R}^d)} \left| \int k(\theta, \theta) \nabla \cdot \nabla_V \mathcal{L}(Q)(\theta) \, dQ(\theta) \right| < \infty$$

$$\sup_{Q \in \mathcal{P}(\mathbb{R}^d)} \left| \iint k(\theta, \vartheta) \nabla_V \cdot \nabla_V \mathcal{L}(\theta)(\vartheta) \, dQ(\theta) dQ(\vartheta) \right| < \infty.$$

Proof. The first claim follows from combining Items 1 and 2. Continuing from Proposition 4, the second variation is

$$\mathcal{L}''(Q)(\theta)(\vartheta) = \sum_{i=1}^n \frac{p_\theta(y_i|x_i) p_\vartheta(y_i|x_i)}{p_Q(y_i|x_i)^2},$$

which is well-defined since, under our assumptions, $p_Q(y_i|x_i) = \int p_\theta(y_i|x_i) \, dQ(\theta)$ is strictly positive for all $Q \in \mathcal{P}(\mathbb{R}^d)$ and all (x_i, y_i) in the dataset. The required variational gradients are

$$\nabla \cdot \nabla_V \mathcal{L}(Q)(\theta) = - \sum_{i=1}^n \frac{\Delta_\theta p_\theta(y_i|x_i)}{p_Q(y_i|x_i)}$$

$$\nabla_V \cdot \nabla_V \mathcal{L}(Q)(\theta)(\vartheta) = \sum_{i=1}^n \frac{\nabla_\theta p_\theta(y_i|x_i) \cdot \nabla_\vartheta p_\vartheta(y_i|x_i)}{p_Q(y_i|x_i)^2},$$

whose terms we assumed to be well-defined. Finally, since each $k(\theta, \theta) \Delta_\theta p_\theta(y_i|x_i)$ is bounded in θ , $k(\theta, \theta) \nabla \cdot \nabla_V \mathcal{L}(Q)$ is Q -integrable for each $Q \in \mathcal{P}(\mathbb{R}^d)$. Likewise, since $|k(\theta, \vartheta)| \leq \sqrt{k(\theta, \theta)} \sqrt{k(\vartheta, \vartheta)}$ and each $\sqrt{k(\theta, \theta)} \nabla_\theta p_\theta(y_i|x_i)$ is bounded in θ , we deduce that $k(\theta, \vartheta) \nabla_V \cdot \nabla_V \mathcal{L}(Q)(\theta)(\vartheta)$ is $Q \otimes Q$ -integrable for each $Q \in \mathcal{P}(\mathbb{R}^d)$. Integrating these equations and applying Jensen's inequality,

$$\left| \int k(\theta, \theta) \nabla \cdot \nabla_V \mathcal{L}(Q)(\theta) \, dQ(\theta) \right| \leq \sum_{i=1}^n \frac{\int k(\theta, \theta) |\Delta_\theta p_\theta(y_i|x_i)| \, dQ(\theta)}{\int p_\theta(y_i|x_i) \, dQ(\theta)}$$

$$\left| \iint k(\theta, \vartheta) \nabla_V \cdot \nabla_V \mathcal{L}(\theta)(\vartheta) \, dQ(\theta) dQ(\vartheta) \right| \leq \sum_{i=1}^n \left(\frac{\int \sqrt{k(\theta, \theta)} \|\nabla_\theta p_\theta(y_i|x_i)\| \, dQ(\theta)}{\int p_\theta(y_i|x_i) \, dQ(\theta)} \right)^2.$$

Let Π_Q denote the distribution for which $(d\Pi_Q/dQ)(\theta) \propto p_\theta(y_i|x_i)$, so that

$$\frac{\int k(\theta, \theta) |\Delta_\theta p_\theta(y_i|x_i)| \, dQ(\theta)}{\int p_\theta(y_i|x_i) \, dQ(\theta)} = \int \underbrace{k(\theta, \theta) \frac{|\Delta_\theta p_\theta(y_i|x_i)|}{p_\theta(y_i|x_i)}}_{(*)} \, d\Pi_Q(\theta)$$

$$\frac{\int \sqrt{k(\theta, \theta)} \|\nabla_\theta p_\theta(y_i|x_i)\| \, dQ(\theta)}{\int p_\theta(y_i|x_i) \, dQ(\theta)} = \int \underbrace{\sqrt{k(\theta, \theta)} \frac{\|\nabla_\theta p_\theta(y_i|x_i)\|}{p_\theta(y_i|x_i)}}_{(**)} \, d\Pi_Q(\theta)$$

where, under our assumptions, both integrands (*) and (**) are bounded over $\theta \in \mathbb{R}^d$. It follows that both integrals are bounded over $\Pi_Q \in \mathcal{P}(\mathbb{R}^d)$, and hence over $Q \in \mathcal{P}(\mathbb{R}^d)$, completing the argument. \square

A.3.3 Proof of Proposition 2

At last we can present a proof of Proposition 2:

Proof of Proposition 2. Our task is to verify the conditions of Theorem 1 for $\mathcal{L} = \mathcal{L}_{\text{PRO}}$:

1. (Integrability) From (13) and the boundedness of $\theta \mapsto p_\theta(y_i|x_i)$ for each (x_i, y_i) , we deduce that $\mathcal{L}'(Q)$ is bounded and thus $\exp(-\mathcal{L}'(Q))$ is integrable with respect to Q_0 .
2. (Loss) Since each $\theta \mapsto p_\theta(y_i|x_i)$ is $C^3(\mathbb{R}^d)$, $(\theta_1, \dots, \theta_N) \mapsto p_{Q_N}(y_i|x_i)$ is $C^3(\mathbb{R}^{d \times N})$. From (12), $(\theta_1, \dots, \theta_N) \mapsto \nabla_V \mathcal{L}(Q_N)(\theta_i)$ is thus also $C^3(\mathbb{R}^{d \times N})$ for each $i \in \{1, \dots, N\}$. Since $\theta \mapsto \nabla_\theta \log p_\theta(y_i|x_i)$ has at most linear growth, from (12)

$$\begin{aligned} |\nabla_V \mathcal{L}(Q_N)(\theta_j)| &= \left| - \sum_{i=1}^n \frac{\nabla_{\theta_j} p_{\theta_j}(y_i|x_i)}{\frac{1}{N} \sum_{r=1}^N p_{\theta_r}(y_i|x_i)} \right| \\ &\leq N \sum_{i=1}^n \left| \frac{\nabla_{\theta_j} p_{\theta_j}(y_i|x_i)}{p_{\theta_j}(y_i|x_i)} \right| = N \sum_{i=1}^n |\nabla_{\theta_j} \log p_{\theta_j}(y_i|x_i)| \end{aligned}$$

has at most linear growth as well. From Proposition 7 both of the integrability conditions on the loss in Item 2 of Theorem 1 are satisfied.

3. (Regularisation) Satisfied by assumption.
4. (Initialisation) Satisfied by assumption.
5. (Kernel) Satisfied by assumption.
6. (Growth) The at most linear growth of $\theta \mapsto k(\theta, \theta) \|\nabla_\theta p_\theta(y_i|x_i)\|$ was established in Proposition 7. The remaining growth requirements were directly assumed.

This completes the argument. \square

A.4 Proof of Proposition 3

This appendix is dedicated to a proof of our final theoretical result:

Proof of Proposition 3. For these calculation we recall that $A : B = \text{tr}(AB^\top)$ for matrices A, B is the double dot product and that $[\nabla_\theta v(\theta)]_{i,j} = \nabla_{\theta_i} v_j(\theta)$ and $[\Delta_\theta v(\theta)]_j = \Delta_\theta v_j(\theta)$

for vector-valued $v : \mathbb{R}^d \rightarrow \mathbb{R}^d$. By convention $v(\theta)$ is a column vector and $\Delta_\theta v(\theta)$ is a row vector for $v : \mathbb{R}^d \rightarrow \mathbb{R}^d$. For the Gaussian location model

$$\begin{aligned} \nabla_\theta p_\theta(y_i|x_i) &= (\nabla_\theta f_\theta(x_i))\Sigma^{-1}(y_i - f_\theta(x_i))p_\theta(y_i|x_i) \\ \Delta_\theta p_\theta(y_i|x_i) &= (\Delta_\theta f_\theta(x_i))\Sigma^{-1}(y_i - f_\theta(x_i))p_\theta(y_i|x_i) \\ &\quad + (\nabla_\theta f_\theta(x_i)) : [\nabla_\theta p_\theta(y_i|x_i)(y_i - f_\theta(x_i))^\top - (\nabla_\theta f_\theta(x_i))p_\theta(y_i|x_i)]\Sigma^{-1} \\ &= \left\{ \begin{array}{l} (\Delta_\theta f_\theta(x_i))\Sigma^{-1}(y_i - f_\theta(x_i)) \\ + (\nabla_\theta f_\theta(x_i)) : [(\nabla_\theta f_\theta(x_i))\Sigma^{-1}(y_i - f_\theta(x_i))(y_i - f_\theta(x_i))^\top \Sigma^{-1}] \\ - (\nabla_\theta f_\theta(x_i)) : [(\nabla_\theta f_\theta(x_i))\Sigma^{-1}] \end{array} \right\} p_\theta(y_i|x_i) \end{aligned}$$

so that

$$\begin{aligned} \sup_{\theta \in \mathbb{R}^d} \sqrt{k(\theta, \theta)} \frac{\|\nabla_\theta p_\theta(y_i|x_i)\|}{p_\theta(y_i|x_i)} &= \sup_{\theta \in \mathbb{R}^d} \sqrt{k(\theta, \theta)} \|(\nabla_\theta f_\theta(x_i))\Sigma^{-1}(y_i - f_\theta(x_i))\| \\ &\leq \|\Sigma^{-1}y_i\| \sup_{\theta \in \mathbb{R}^d} \sqrt{k(\theta, \theta)} \|(\nabla_\theta f_\theta(x_i))\|_{\text{op}} \\ &\quad + \|\Sigma^{-1}\|_{\text{op}} \left[\sup_{\theta \in \mathbb{R}^d} \|f_\theta(x_i)\| \right] \left[\sup_{\theta \in \mathbb{R}^d} \sqrt{k(\theta, \theta)} \|(\nabla_\theta f_\theta(x_i))\|_{\text{op}} \right] \end{aligned}$$

where the finiteness of the terms appearing on the right hand side was assumed. A similar but more lengthy calculation (which we omit for brevity) for the second supremum completes the argument. \square

B Experimental Protocol

This appendix contains the details required to reproduce the experiments reported in Section 3. The test problems that we consider are specified in Section B.1, details of the maximum mean discrepancy test statistic are contained in Section B.2, implementational aspects of VGD are discussed in Section B.3, and additional empirical results are contained in Section B.4. Full details for the seismic travel time tomography case study are contained in Section B.5.

Code Code to reproduce our simulation study from Section 3.1 is available at <https://github.com/liuqingyang27/Detecting-Model-Misspecification-via-VGD>. Code to reproduce our seismic travel time tomography experiments from Section 3.2 is available at <https://github.com/XuebinZhaoZXB/Detecting-Model-Misspecification/>.

B.1 Test Problems

The regression functions that we considered for our simulation study in Section 3.1 are as follows:

1. $f_\theta(x) = \theta x^2$ with $\theta \in \mathbb{R}$ and $\{x_i\}$ uniformly sampled from $[0, 1]$

2. $f_\theta(x) = \frac{1}{1+e^{-\theta x}}$ with $\theta \in \mathbb{R}$ and $\{x_i\}$ uniformly sampled from $[-1, 1]$
3. $f_\theta(x) = \theta_1 + \theta_2 x$ with $\theta \in \mathbb{R}^2$ and $\{x_i\}$ uniformly sampled from $[-2, 2]$

In the well-specified scenario, data are generated by $y_i = f_\theta(x_i) + z_i$ for all $i \in \{1, \dots, n\}$, where z_i are i.i.d $\mathcal{N}(0, \sigma^2)$. For the three cases above, the noise levels are separately 0.5, 0.05 and 0.8. The true data-parameters parameters in this case were $\theta = 5$ for the quadratic model, $\theta = 5$ for the sigmoid model and $\theta = [5, 3]$ for the linear model. To generate data that are misspecified we proceeded as follows for each of the above tasks:

1. $y_i = (5 + 3u_i)x_i^2 + z_i$ for all $i \in \{1, \dots, n\}$, where $u_i \sim \mathcal{N}(0, 1)$, $z_i \sim \mathcal{N}(0, 0.5^2)$
2. data points are generated from a uniform distribution with density

$$f(x, y) = \begin{cases} \frac{1}{2}, & \text{if } (x, y) \in (0, 1) \times (0, 1), \\ \frac{1}{2}, & \text{if } (x, y) \in (-1, 0) \times (-1, 0), \\ 0, & \text{otherwise.} \end{cases}$$

3. $y_i = 5 + 3x_i + 2x_i^2 + z_i$ for all $i \in \{1, \dots, n\}$, where $z_i \sim \mathcal{N}(0, 0.8^2)$.

In the second of the above examples $\theta \mapsto f_\theta(x)$, $\nabla_\theta f_\theta(x)$ and $\Delta_\theta(x)$ are bounded, so from Proposition 3 the sufficient conditions of our theory are satisfied whenever the kernel k is bounded. On the other hand, in the first and third cases our theoretical assumptions are *not* satisfied; this enables us to test the performance of Algorithm 1 outside the setting where our theoretical results hold.

B.2 Maximum Mean Discrepancy

The maximum mean discrepancy employed in these experiments utilised a Gaussian kernel

$$\exp\left(-\frac{\|y - y'\|^2}{2\ell^2}\right)$$

where the lengthscale was selected as the standard deviation of $\{y_i\}_{i=1}^n$. For the synthetic examples we present in Section 3.1, the dimension of the response variable is always $p = 1$, but for completeness here we work with the general form of the Gaussian kernel. The choice of a Gaussian kernel together with the Gaussian measurement error model (11) with covariance matrix $\Sigma = \sigma^2 I_{p \times p}$ enables (10) to be explicitly computed using the analytic form of the integral

$$\begin{aligned} \kappa(\theta, \vartheta | x_i) &:= \iint \exp\left(-\frac{\|y - y'\|^2}{2\ell^2}\right) dP_\theta(y|x_i) dP_\vartheta(y'|x_i) \\ &= \left(\frac{\ell^2}{\ell^2 + 2\sigma^2}\right)^{p/2} \exp\left(-\frac{\|f_\theta(x_i) - f_\vartheta(x_i)\|^2}{2(\ell^2 + 2\sigma^2)}\right) \end{aligned}$$

together with

$$\begin{aligned} \text{MMD}^2(P_{\text{Bayes}}(\cdot|x_i), P_{\text{PrO}}(\cdot|x_i)) &= \iint \kappa(\theta, \vartheta|x_i) \, dQ_{\text{Bayes}}(\theta) dQ_{\text{Bayes}}(\vartheta) \\ &\quad - 2 \iint \kappa(\theta, \vartheta|x_i) \, dQ_{\text{Bayes}}(\theta) dQ_{\text{PrO}}(\vartheta) \\ &\quad + \iint \kappa(\theta, \vartheta|x_i) \, dQ_{\text{PrO}}(\theta) dQ_{\text{PrO}}(\vartheta). \end{aligned} \quad (18)$$

In practice both Q_{Bayes} and Q_{PrO} are approximated using VGD, so we obtain a particle-based representation $\{\theta_i^{\text{Bayes}}\}_{i=1}^N$ for Q_{Bayes} and $\{\theta_i^{\text{PrO}}\}_{i=1}^N$ for Q_{PrO} . Substituting these empirical measures into (18) we obtain

$$\begin{aligned} \text{MMD}^2(P_{\text{Bayes}}(\cdot|x_i), P_{\text{PrO}}(\cdot|x_i)) &\approx \frac{1}{N^2} \sum_{r=1}^N \sum_{s=1}^N \kappa(\theta_r^{\text{Bayes}}, \theta_s^{\text{Bayes}}|x_i) \\ &\quad - 2 \frac{1}{N^2} \sum_{r=1}^N \sum_{s=1}^N \kappa(\theta_r^{\text{Bayes}}, \theta_s^{\text{PrO}}|x_i) \\ &\quad + \frac{1}{N^2} \sum_{r=1}^N \sum_{s=1}^N \kappa(\theta_r^{\text{PrO}}, \theta_s^{\text{PrO}}|x_i). \end{aligned} \quad (19)$$

The approximate values in (19) were used for the experiments that we report in Section 3 of the main text.

B.3 Variational Gradient Descent

For our toy experiments we utilised the inverse multiquadric kernel

$$k(x, y) = \left(c^2 + \frac{\|x - y\|^2}{l^2} \right)^{-\beta}$$

with $\beta = 0.5$. To select an appropriate length scale l , we employed the median heuristic [Garreau et al., 2017] at each iteration of Algorithm 1. The step size and iteration number in each experiment were manually selected to ensure convergence, as quantified by KGD (see e.g. Figure 5). In all experiments $N = 20$ particles were used.

B.4 Additional Empirical Results

The posterior distributions Q_{Bayes} and Q_{PrO} corresponding to the regression tasks in Figure 2 are displayed in Figure 5, alongside the values of the KGD in (9) obtained along the trajectory of VGD. A kernel density estimator has been applied to the particle representations of Q_{Bayes} and Q_{PrO} to aid visualisation in Figure 5. It can be seen that the standard Bayesian posterior Q_{Bayes} is rather concentrated in all scenarios, irrespective of whether the statistical model

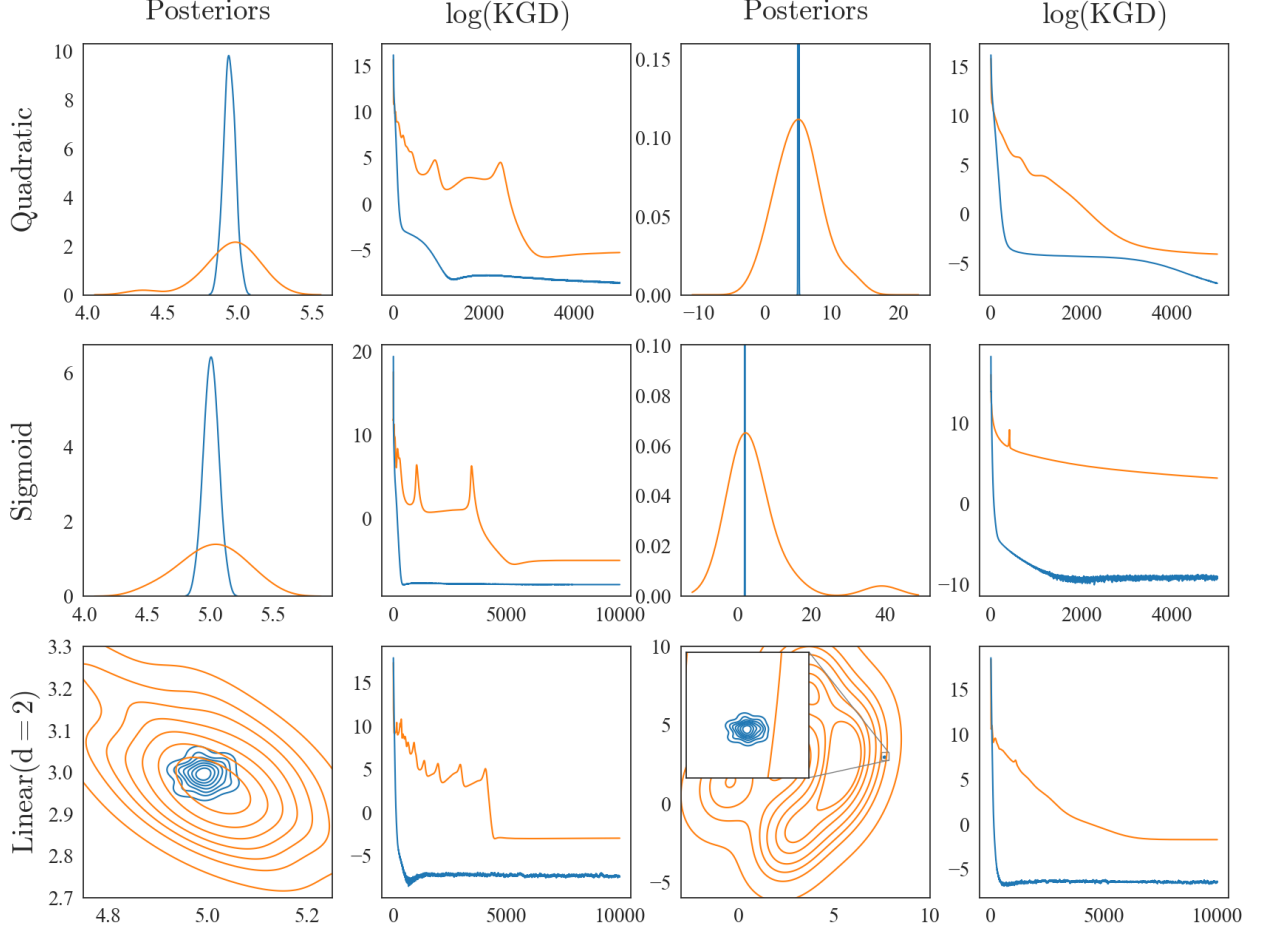


Figure 5: Simulation Study. Each row corresponds to a regression task in Figure 2 in which the data are either generated from the statistical model (well-specified, left) or not generated from the statistical model (misspecified, right). The posterior distributions Q_{Bayes} (blue) and Q_{Pro} (orange) are displayed, together with the values of the KGD in (9) obtained along the trajectory of VGD.

is well-specified or misspecified, while Q_{Pro} tends to be more diffuse when the statistical model is misspecified. The values of KGD obtained along the trajectory of VGD appear to generally decrease and converge to a limit in all cases, consistent with an accurate N -particle approximation having been found.

Further to the analysis in the main text, we investigate the performance of our method under different data sizes n and different dimensions of θ .

First, in Figure 6, we considered the sigmoid regression task with varying sample sizes of $n = 100, 1000$ and 10000 . The MMD values $D(\{(x_i, \tilde{y}_i)\}_{i=1}^n)$ calculated under the null typically decrease as the data size grows, while under misspecification the actual MMD values are effectively n -independent. Consequently, misspecified models are easier to detect when we have a larger dataset, as would be expected.

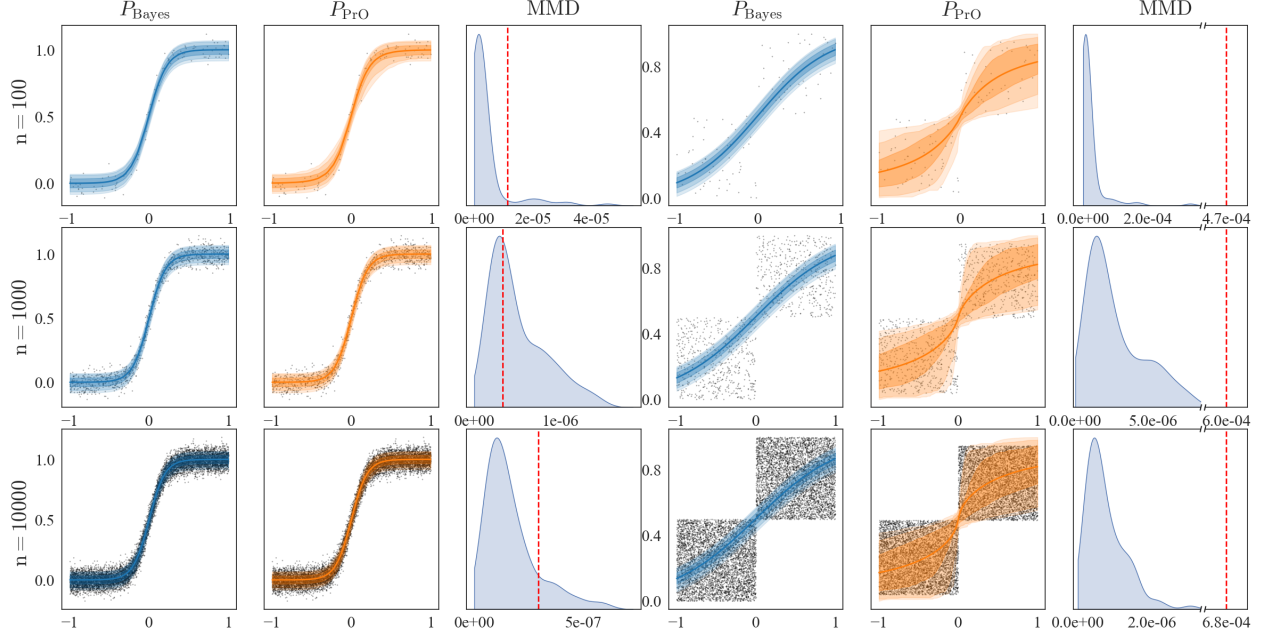


Figure 6: Additional simulation study, varying the size n of the dataset. Each row corresponds to the sigmoid regression task in Figure 2 with different data sizes in which the data are either generated from the statistical model (well-specified, left) or not generated from the statistical model (misspecified, right). The posterior predictive distributions P_{Bayes} and P_{PrO} are displayed, along with the null distribution under the hypothesis that the statistical model is well-specified, and actual realised value of the test statistic D in (10) (red dashed).

Second, in Figure 7 we consider a regression model defined by

$$f_{\theta}(x) = \sum_{p=1}^d \theta_p \sin(px). \quad (20)$$

For the misspecified scenario, the data are generated according to $y_i = \sin(1/x_i) + z_i$ where $z_i \sim \mathcal{N}(0, \sigma^2)$ and $\sigma = 0.2$, a function that remains misspecified regardless of the dimension p of the model (20). In particular, we cannot expect (20) to resolve the rapid oscillations around $x = 0$. For presentational purposes we consider $p \in \{5, 20, 50\}$. The predictive distributions P_{Bayes} and P_{PrO} perform generally well when the model is well-specified. In the misspecified case, P_{Bayes} is over-confident around $x = 0$ and this is partially remedied in P_{PrO} . The power of diagnostic declines with increasing parameter dimension p , as the actual MMD value gets closer to the effective support of the null; however, the test still had power to reject the well-specified null even when $p = 50$.

In summary, our additional experiments confirm the intuition that larger dataset sizes n increase our power to detect when the model is misspecified, while larger parameter dimension p decreases our power to detect when the model is misspecified.

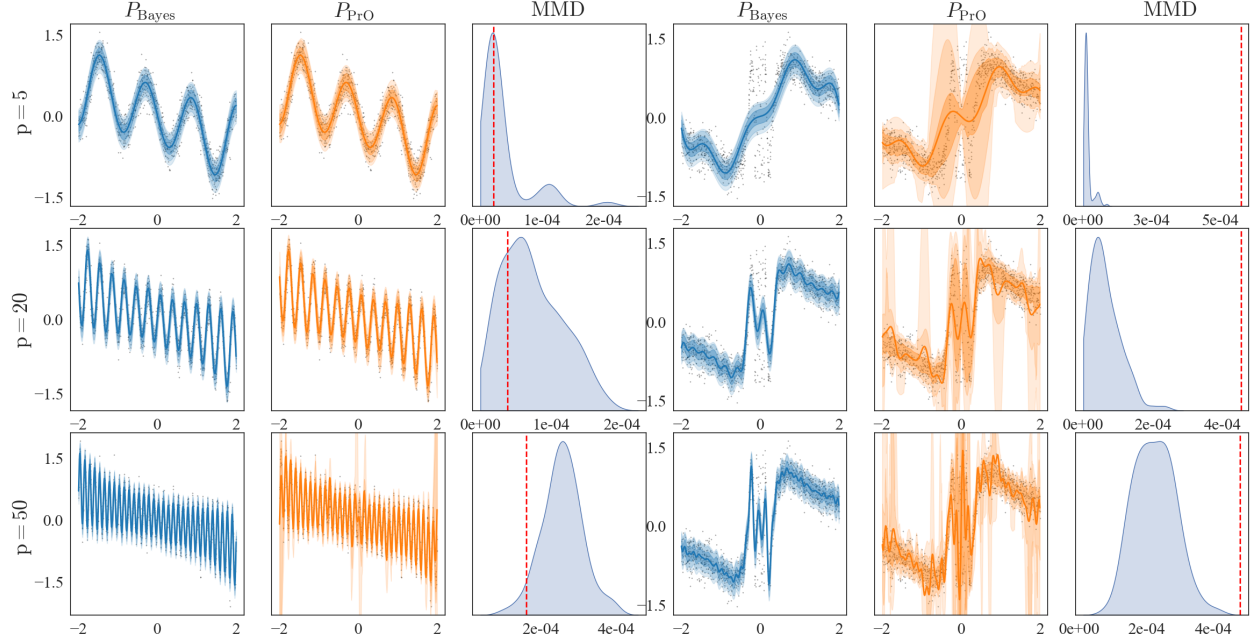


Figure 7: Additional simulation study, varying the number p of parameters in the model. Each row corresponds to a regression task using model (20) with different parameters dimension, in which the data are either generated from the statistical model (well-specified, left) or not generated from the statistical model (misspecified, right). The posterior predictive distributions P_{Bayes} and P_{PrO} are displayed, along with the null distribution under the hypothesis that the statistical model is well-specified, and actual realised value of the test statistic D in (10) (red dashed).

B.5 Details for Seismic Travel Time Tomography

For computation using VGD, a set of $N = 600$ particles $\{\theta_j^0\}_{j=1}^N$ were initialised by sampling from the prior Q_0 . A total of $T = 500$ iterations of VGD were performed with step size $\epsilon = 0.1$. The Gaussian kernel was used, in line with earlier work in this context, and the length scale was calculated by the median of pairwise distances between particles [Garreau et al., 2017].